Remote Sensing of Environment 310 (2024) 114230

Contents lists available at ScienceDirect

Remote Sensing of Environment

journal homepage: www.elsevier.com/locate/rse

Mapping the successional stages of biological soil crusts at 3-m resolution in the Gurbantunggut Desert, China through hydration-induced spectral response

Ruilin Chen [a,1], Benfeng Yin [b,1], Wei Yang [c], Jianlong Li [a], Zeteng Li [a], Yuanming Zhang [b,*], Jin Chen [a,*]

[a] State Key Laboratory of Remote Sensing Science, Faculty of Geographical Science, Beijing Normal University, Beijing 100875, China
[b] State Key Laboratory of Desert and Oasis Ecology, Key Laboratory of Ecological Safety and Sustainable Development in Arid Lands, Xinjiang Institute of Ecology and Geography, Chinese Academy of Sciences, 830011 Urumqi, China
[c] Center for Environmental Remote Sensing, Chiba University, Chiba 2638522, Japan

ARTICLE INFO

Editor: Marie Weiss

Keywords:
Biological soil crusts
Successional stages
Hydration events
Spectral response
Random forest (RF) model

ABSTRACT

Biological soil crusts (biocrusts) are essential components of desert ecosystems and provide diverse ecological services that benefit both the environment and human society. Biocrusts exhibit varying ecological functions as they pass through several successional stages—cyanobacteria, lichens, semi-mosses, and mosses. Remote sensing has been widely applied to monitor the spatial and temporal distributions of biocrusts. However, previous efforts have focused primarily on identifying biocrusts while disregarding their distinct successional stages. Additionally, biocrusts remain dormant or inactive for most of the year, resulting in biocrusts at different successional stages with similar spectral characteristics, making them challenging to distinguish. Fortunately, biocrusts at different successional stages exhibit distinct spectral responses to hydration events. By leveraging imagery with high temporal (1-day) and spatial (3-m) resolutions from the PlanetScope constellation, this study attempts to map biocrust successional stages on a regional scale using transient spectral responses induced by a snowmelt event. We employed a two-stage mapping framework utilizing the random forest (RF) model. The aim of the first stage was to identify biocrusts, while the second stage was focused on mapping their distinct successional stages. The results showed that snowmelt induces noticeable changes in biocrust spectra, helping to distinguish between biocrusts and other background components and among different stages of biocrust succession. Our mapping framework achieved overall accuracies of 0.96 (252 out of 263 correctly identified samples) and 0.8 (85 out of 106 correctly identified) in the above two stages, respectively, highlighting its ability to delineate spatial patterns of successional stages across landscape and regional scales. This study lays a foundation for future in-depth exploration of desert ecosystem dynamics, including structure, ecological services, and responses to climate change and human activities. Furthermore, we suggest that event-induced spectral responses could improve classification accuracy, especially when spectral features are similar under general conditions.

1. Introduction

Biological soil crusts (biocrusts) are widely distributed in desert areas worldwide and are complex mixtures of soil granules and microscopic organisms such as cyanobacteria, algae, fungi, and bacteria, as well as macroscopic entities such as lichens and mosses (Belnap et al., 2016). Despite their inconspicuous nature, biocrusts provide diverse ecological services that benefit both the environment and human society, including increasing resistance to wind erosion (Belnap and Gillette, 1998; Belnap et al., 2014; Eldridge and Leys, 2003; Hamid Lajevardi and Shafiei, 2023) and water erosion (Colica et al., 2014; Gao et al., 2020a, 2020b; Knapen et al., 2007; Rabiei et al., 2022; Zhao et al., 2014); improving soil fertility through carbon and nitrogen fixation (Sancho et al., 2016); influencing plant germination and growth (Bowker et al., 2022; Li et al., 2005; Rivera-Aguilar et al., 2005); and providing habitat for a variety of insect species (Li et al., 2006). On the

* Corresponding authors.
E-mail addresses: zhangym@ms.xjb.ac.cn (Y. Zhang), chenjin@bnu.edu.cn (J. Chen).
[1] These two authors contributed equally to the study.

https://doi.org/10.1016/j.rse.2024.114230
Received 4 January 2024; Received in revised form 25 April 2024; Accepted 26 May 2024
Available online 30 May 2024

other hand, biocrusts are highly vulnerable to climate change and physical disturbance (Escolar et al., 2012; Ferrenberg et al., 2015; Rodríguez-Caballero et al., 2018; Phillips et al., 2022). Furthermore, biocrusts exhibit a slow recovery process, with full recovery from physical disturbances potentially taking several decades (Deng et al., 2020; Weber et al., 2016). Given their critical ecological significance and vulnerability, a reliable technique for mapping both the spatial distribution and temporal dynamics of biocrusts is imperative.

Biocrust distribution is typically investigated in three ways: field surveys, predictive modeling, and remote sensing mapping. While field surveys are nominally the most reliable approach, they are time consuming, labor intensive, and limited to accessible areas (Wu and Zhang, 2013). Conversely, predictive models offer a pragmatic approach for regional-scale estimation (Beaugendre et al., 2017; Bowker et al., 2006; Bu et al., 2016; Qiu et al., 2023; Rodríguez-Caballero et al., 2018). However, these methods generally estimate potential rather than actual distribution areas; they also rely on the availability of environmental data and are limited by both the spatial resolution and the quality of such data. For instance, soil and climate data typically have spatial resolutions of 0.25 to 10 km and are less reliable in desert areas due to the scarcity of meteorological and hydrological stations (Qiu et al., 2023; Rodríguez-Caballero et al., 2018; Chen et al., 2023). Fortunately, advances in remote sensing have provided unprecedented opportunities for regional biocrust mapping (Smith et al., 2019). Currently, two primary methods have emerged: index-based and machine learning (ML)-based approaches. For the index-based approach, Karnieli (1997) formulated a Crust Index (CI) for mapping cyanobacteria-dominated biocrusts based on a notable increase in the blue spectral band due to the presence of phycobilin pigment in the biocrust type. Chen et al. (2005) further developed the Biological Soil Crust Index (BSCI) for mapping lichen-dominated biocrusts by exploiting the spectral flatness from the green to red bands and the darkness in the visible and near-infrared bands of biocrust types. Recently, Wang et al. (2022) developed two indices, the Sandy Land Ratio Crust Index (SRCI) and the Desert Ratio Crust Index (DRCI), to identify moss-dominated and lichen-dominated biocrusts. However, the information derived from individual indices is inherently limited. To address this issue, ML models have been introduced to take full advantage of multiple spectral features, with promising results using Support Vector Machine (SVM) in biocrust mapping (Collier et al., 2022; Havrilla et al., 2020; Rodríguez-Caballero et al., 2014). Although recent research has significantly advanced the power of biocrust mapping, most related efforts have concentrated on mapping biocrusts at specific successional stages (i.e., cyanobacteria, lichens, or mosses), and comprehensive mapping of biocrust succession is still lacking.

Biocrusts exhibit various successional stages (Belnap et al., 2008) (Fig. 1). In a typical successional sequence, cyanobacteria and algae initiate the colonization of the soil surface, facilitating carbon and nitrogen fixation to establish a stable, nutrient-rich substrate. Subsequently, lichen coverage expands, often accompanied by the emergence of mosses. In an undisturbed environment with suitable soil properties, temperature, radiation, and sufficient water and nutrient resources, mosses eventually dominate biocrust communities, marking the final successional stage (Lan et al., 2012, 2013; Weber et al., 2016). Transitioning through these stages, biocrusts exhibit varying ecological functions, i.e., different capacities for nutrient fixation and erosion resistance (Chamizo et al., 2012a; Housman et al., 2006; Yang et al., 2022). Moreover, their successional status also serves as a bioindicator of ecosystem change due to their susceptibility to environmental stress and disturbance (Belnap et al., 2013; Chamizo et al., 2012b; Holt and

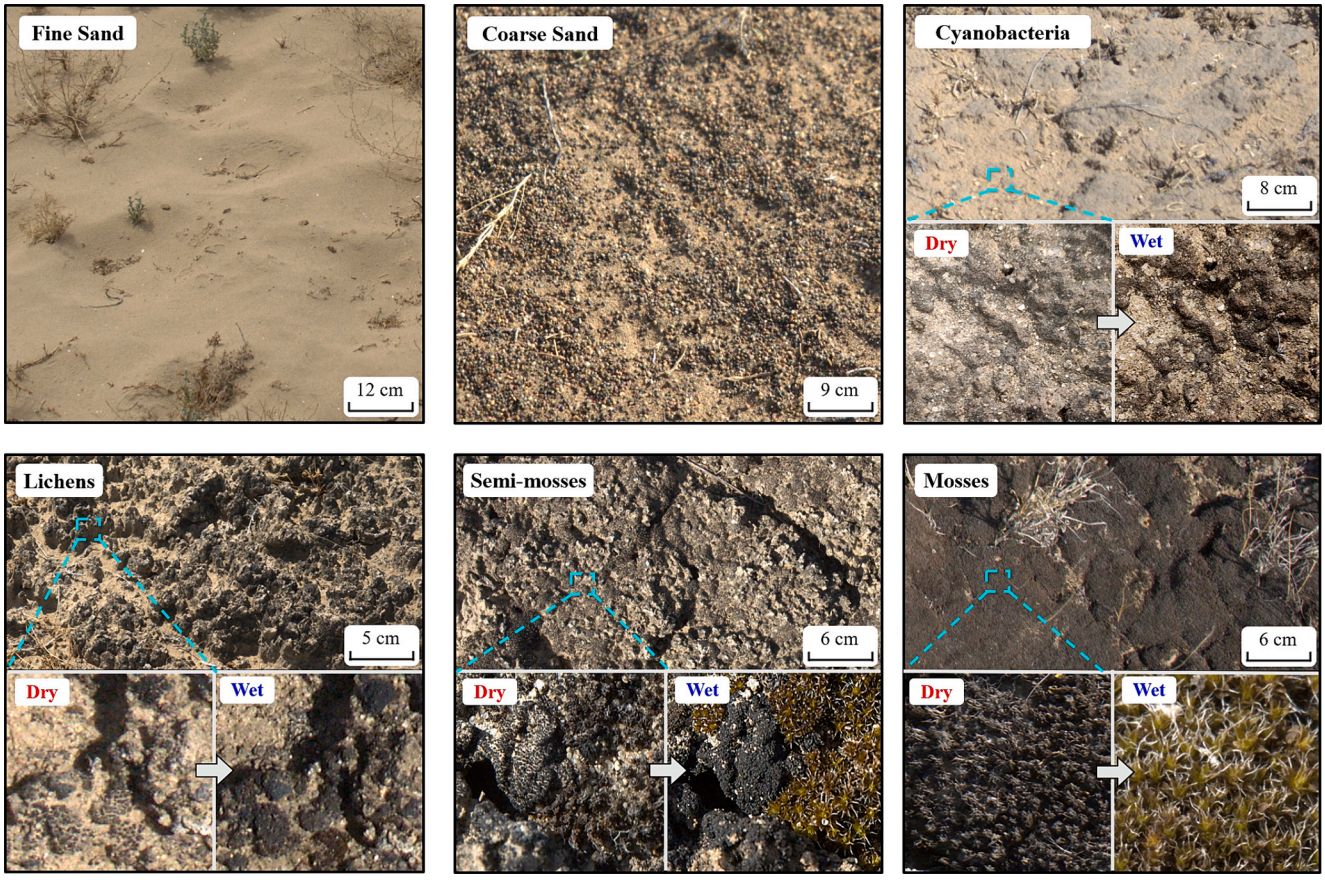

Fig. 1. Ground-level photographs of biocrusts at different successional stages and common land cover types in the Gurbantunggut Desert. These photos were taken in July 2023. Subplots for each biocrust depict its appearance before and after a hydration event.

Miller, 2010; Phillips et al., 2022). Therefore, mapping biocrust succession is essential for a comprehensive study of desert ecosystem dynamics, including structure, ecological services, and responses to climate change and human intervention. However, biocrust succession mapping is not straightforward, as the spectra have similar profiles (Wang et al., 2023; Yamano et al., 2006), with nuances detectable only in narrow-band absorptions induced by specific pigments such as chlorophyll *a* (Lan et al., 2012) and carotenoids (Reuter and Müller, 1993). Consequently, differentiating between successional stages relies heavily on hyperspectral data, which severely limits the practicality of these methods, although promising results have been achieved in mapping cyanobacteria and lichens using hyperspectral imagery (Rodríguez-Caballero et al., 2014).

Fortunately, biocrusts at different successional stages exhibit distinct spectral responses to hydration events (i.e., rainfall, fog and snowmelt) (Wang et al., 2023; Yamano et al., 2006) (Fig. 1). Following hydration events, late-stage biocrusts (e.g., mosses) exhibit darker (i.e., lower reflectance) and greener (i.e., increased red light absorption) appearances than early-stage biocrusts (e.g., cyanobacteria) due to their greater water-holding capacity (Yair et al., 2011) and higher photosynthetic biomass content (Proctor and Smirnoff, 2000; Lan et al., 2019). Despite this clear distinction, few studies have exploited this feature in biocrust succession mapping due to two major challenges. First, symbiotic relationships are common within biocrust communities, resulting in considerable heterogeneity and mixing of biocrust communities even at the patch scale (Lan et al., 2019). This heterogeneity, coupled with the mixed pixel effect due to the limited spatial resolution (>10 m) of most wide-area imaging satellites, poses challenges in mapping biocrust successional stages at coarser spatial resolutions. Second, the harsh desert environment rapidly dehydrates biocrusts after hydration events, typically within <24 h (Chen et al., 2023), significantly limiting the duration of observable spectral responses. Recently, Planet, a commercial enterprise with >200 CubeSats in orbit, has provided the opportunity to acquire images with unprecedented temporal (1 day) and spatial (3 m) resolution (Planet Team, 2017). This increased observational capacity enables the fine-scaled capture of spectral response intensities following hydration events within a 24-h period, which presents a promising avenue for biocrust succession mapping based on the distinct spectral responses of biocrusts at different successional stages to hydration events.

Accordingly, we hypothesize that biocrust succession mapping may be feasible if the spectral responses of biocrusts to hydration events can be observed by high spatial-temporal resolution satellite sensors. We evaluated this hypothesis by conducting a case study in the Gurbantunggut Desert, China. Our study was driven by three main objectives: 1) To identify a suitable hydration event that would hydrate biocrusts in a uniform and complete manner across the desert. 2) To quantify the distinct spectral responses of different successional stages of biocrusts. 3) To map biocrust succession through the use of spectral responses induced by a hydration event in a random forest (RF) model.

2. Study area and data

2.1. Study area

The Gurbantunggut Desert is the largest mobile and stabilized sandy desert in China; it is located in the transition zone between Central and East Asia (85–90°E, 44–47°N) and has an area of approximately 4.88 × 10^4 km^2 (Fig. 2(a)). The landscape is characterized by large and densely populated stabilized sand dunes, typically 30 to 50 m high (Li et al., 2022), interspersed with sparse vegetation (e.g., *Haloxylon ammodendron*). Open spaces are often covered by biocrusts, with late-stage biocrusts such as mosses (e.g., *Syntrichia caninervis*) and lichens (e.g., *Collema tenex*) dominating the interdune areas, while early-stage

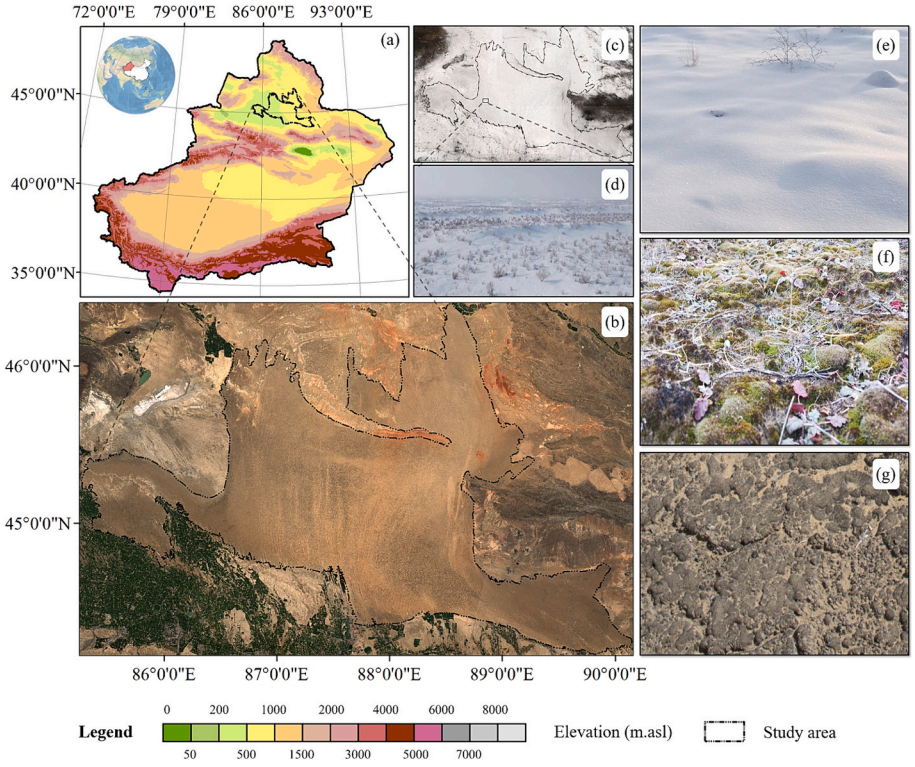

Fig. 2. (a) Location of the study area (elevation data: GMTED2010) and (b) the summer landscape of the Gurbantunggut Desert shown in Sentinel-2 imagery acquired during June 2023 and (c) the winter landscape of the Gurbantunggut Desert shown in Sentinel-2 imagery acquired during February 2023 and (d) an aerial image of a typical sand dune landscape in winter. (e) – (g) Representation of three distinct periods in the Gurbantunggut Desert throughout the year: a snow cover period from December to February, a snowmelt event in early to mid-March, and an arid period from April to October. These photos were taken in 2023. (For interpretation of the references to colour in this figure legend, the reader is referred to the web version of this article.)

biocrusts such as cyanobacteria (e.g., *Microcoleus paludosus*) and algae (e.g., *Chlorella vulgaris*) occur on sand dune slopes (Zhang et al., 2010). Under a typical continental arid climate, the annual precipitation ranges from 80 to 150 mm (statistics from 2006 to 2020), falling predominantly during winter and spring. The average annual temperature varies between 6 and 10 °C (statistics from 2006 to 2020), with the maximum summer temperature exceeding 40 °C.

Throughout a year, the Gurbantunggut Desert typically experiences three periods: a three-month period covered by snow from December to February (Fig. 2(e)); a quick snowmelt event lasting approximately one week in early to mid-March (Fig. 2(f)); and ultimately a lengthy arid period from April to October with sparse precipitation (Fig. 2(g)). During the snow-covered period (Fig. 2(c) – (e)), snow depths typically range from 20 to 30 cm, accounting for approximately 30% of the annual precipitation (Zhou et al., 2010). Vertical infiltration is the primary hydrological process during snowmelt events (Hu et al., 2015). This snowmelt process ensures uniform and thorough hydration of the biocrusts, maintaining their biological activity for one week. In addition, while snowmelt can also nourish ephemeral plant growth, the green-up of ephemeral plants usually occurs a few weeks later (Wang, 1993) and thus does not interfere with observations of biocrusts during snowmelt events.

2.2. Data collection and preprocessing

2.2.1. Ground truth data

Ground truth data, including various georeferenced plots of biocrusts at different successional stages (i.e., cyanobacteria, lichens and mosses) and non-biocrust backgrounds (i.e., coarse and fine sand), were collected during a field survey conducted from July 13 to 25, 2023. Fig. 3 illustrates the survey process. Sample sites were selected every 10 km along the desert highway (i.e., 46 sites in total), each representing a typical sand dune landscape, including dune ridges, slopes (i.e., 10 to 40-m areas alongside ridges), and interdune areas. Several plots (i.e., ranging from 15 to 25) were randomly selected within each site. Each plot covered an area of 6 × 6 m and was oriented northward to simplify the calculation of the weighted mean for intersecting pixels. The location of the northwest (NW) point was measured for each plot by three independent portable GPS devices with a positional precision of <1.48 m. Subsequently, an orthographic image with 1 mm spatial resolution was obtained for each plot using an unmanned aerial vehicle (DJI Mini 3 Pro). To determine the coverage of different components, including mosses, lichens, cyanobacteria, fine sand, coarse sand, plants, and plant litter, Support Vector Machine (SVM) was applied to each aerial image. To this end, multiple ground-level photographs were captured from different perspectives using a digital camera (EOS M50 Mark II). Subsequently, three microbiologists performed a double-check of the component coverage estimation using both the aerial and ground-level photographs, as detailed in Appendix S1. Finally, a total of 314 biocrust plots (with biocrust coverage >20%) and 479 non-biocrust plots were used in the two-stage mapping framework. The biocrust plots were categorized into four successional stages following Lan's research (see Section 3.1 for details): cyanobacteria (number of survey plots: 25), lichens (167), semi-mosses (97), and mosses (25). The non-biocrust plots were categorized into two classes based on grain size: fine sand (302) and coarse sand (177).

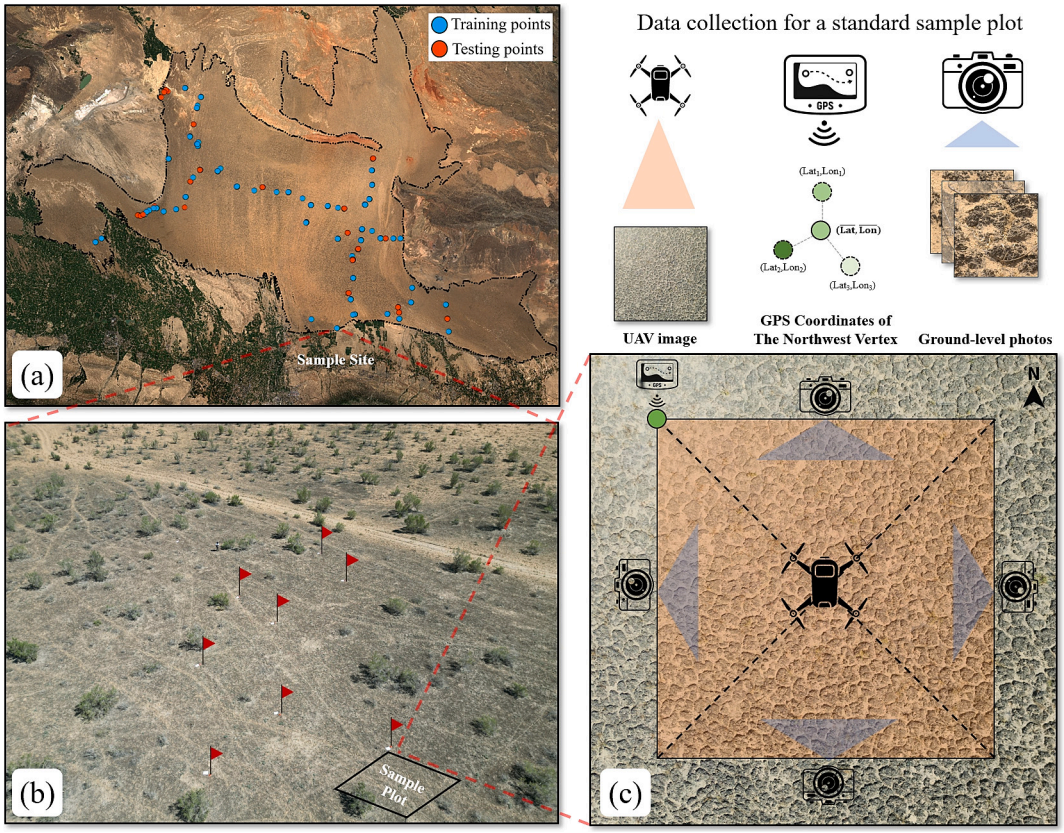

Fig. 3. Illustration of the field survey process. (a) Distribution of the sample sites. The red and blue points refer to the field survey points used as training and test sets for classification, respectively. Both sets are spatially independent. (b) Partial sample plots of a site, with the red flag representing the northwest corner of each plot. (c) Data collection for a standard sample plot, including a high-resolution UAV image (denoted as a 6 × 6 m translucent orange rectangle), averaged GPS coordinates (denoted as a green circle with a solid border) of the northwest corner of the plot from three independent GPS devices (denoted as three green circles with dotted borders), and multiple ground-level photographs taken from different perspectives. (For interpretation of the references to colour in this figure legend, the reader is referred to the web version of this article.)

2.2.2. Remotely sensed data

The PlanetScope constellation offers imagery with remarkable temporal (1 day) and spatial resolution (3.7 to 4.1 m, altitude dependent). This study used PlanetScope Ortho Analytic 8B Surface Reflectance (PSOA8BSR) data with eight spectral bands (Table 1), which is a Level 3B product that has undergone several preprocessing procedures, including radiometric calibration, atmospheric correction, geometric correction, and orthorectification. The processed images achieved an orthorectified pixel size of 3 m and exhibited a colour depth of 16 bits per band. In this study, PSOA8BSR images of both the snowmelt period (i.e., March 10th, 11th, 12th, and 15th of 2023 when biocrusts were wet) and arid period (i.e., September 16th and 17th of 2022 when biocrusts were dry) were obtained from https://www.planet.com/. The images used from both periods were clear of clouds and haze and were acquired under comparable lighting conditions (i.e., solar and viewing angles) (Table 2). Only images classified as "standard" in the "quality category" and pixels flagged as "clear" were retained to ensure observation quality. No evident geometric mismatches were observed among the images. A total of 3023 images were collected for this study. Images acquired by the same satellite on the same day were then mosaiced into strips. In addition, PSOA8BSR images were also collected throughout the year over our sample sites to investigate the variation in biocrust spectra (see Fig. 4 and Fig. 12).

Many studies have reported significant radiometric inconsistency among PlanetScope constellation images due to discrepancies in spectral response function and radiometric quality across different sensors (Frazier and Hemingway, 2021; Houborg and McCabe, 2018; Kington and Collison, 2022; Latte and Lejeune, 2020). To address this issue, previous studies have attempted to rectify PSOA8BSR imagery by referencing globally consistent observations acquired by Landsat 8 (Houborg and McCabe, 2018) or Sentinel 2 (Kington and Collison, 2022). However, these methods address only four out of the eight PSOA8BSR bands (i.e., the blue, green II, red and NIR bands), leaving notable radiometric inconsistencies in the remaining bands (i.e., coastal blue, green I, yellow and red edge bands). To address this, we employed an invariant object-based method to mitigate radiometric inconsistencies among strips (see Appendix S2). Then, the harmonized strips obtained on the same day were mosaiced together, resulting in a collection of six images, one image per day (i.e., two images during the dry period and four images during the snowmelt period). In addition, Scene Classification Maps (SCL) were acquired from Sentinel-2 MSI data collected in February 2023 to identify snow-covered areas. The pixels labeled '11' indicate the presence of snow and were subsequently subjected to the mapping procedure.

3. Methodology

3.1. Defining successional stages of biocrusts and their spectral response to hydration events

Biocrusts exhibit several successional stages under different environmental conditions (i.e., climate, soil microenvironment and physical disturbance), resulting in diverse physiological and ecological characteristics (Belnap et al., 2008). Lan et al. (2013) quantitatively demarcated biocrust succession into stages of cyanobacteria, lichens, semi-mosses and mosses (Fig. 1) utilizing clustering analysis that incorporated multiple biological indicators (Lan et al., 2013). Their demarcation revealed clear differences in community structure and physicochemical characteristics among biocrusts at different successional stages. Therefore, this study adopted the category system. In addition, sands of different grain sizes provide a native background for different successional stages. We also included coarse and fine sand (as defined by ISO 14688-1:2017) in the biocrust succession categories because different sand grain sizes have different degrees of spectral similarity to biocrusts. Table 3 summarizes the definitions of the biocrust succession categories in the study.

Due to the arid environment in the Gurbantunggut Desert, which has an aridity index of 0.10 (Zomer et al., 2022), biocrusts remain dormant or inactive for most of the year, resulting in biocrusts at different successional stages with similar spectral characteristics. However, following a hydration event (e.g., snowmelt, or rainfall), biocrusts at different successional stages exhibit distinct spectral responses, particularly in the following two aspects: darkening (i.e., reduced reflectance while maintaining spectral flatness between the green and red bands) and greening (i.e., increased red light absorption) (Wang et al., 2023; Yamano et al., 2006). Accordingly, this study used two spectral indices, the Biological Soil Crust Index (BSCI) (Chen et al., 2005) and the Red Band Depth (RBD) (Mutanga and Skidmore, 2004), to highlight the darkening and greening response of biocrusts at different successional stages to a hydration event. The BSCI quantifies spectral darkness in the visible and near-infrared bands and flatness from the green to red bands and is expected to increase after hydration (Eq. 1). The RBD quantifies photosynthetic intensity by measuring the depth of the red-light absorption valley, and this parameter is also expected to increase after hydration (Eqs. 2 and 3). In comparison to the Normalized Difference Vegetation Index (NDVI), the Red Band Depth (RBD) exhibits greater resilience against the influence of soil background (Zeng et al., 2022), and has been demonstrated effective in the analysis of both hyperspectral and multispectral data, particularly in identifying subtle spectral variations resulting from increased photosynthetic activity (Panigada et al., 2019).

$$BSCI = \frac{1 - L \times \left| R_{red} - R_{green} \right|}{R^{mean}_{GRNIR}} \quad (1)$$

$$RBD = 1 - \frac{R_{red}}{R^{envelope}_{Red}} \quad (2)$$

$$R^{envelope}_{Red} = \frac{R_{NIR} - R_{green}}{CW_{NIR} - CW_{green}} \times \left(CW_{red} - CW_{green} \right) + \mathrm{R}_{green} \quad (3)$$

Table 2
PSOA8BSR images used in the study.

Acquisition Date	Cloud cover (%)	Heavy haze percent (%)	Sun azimuth (degree)	Sun elevation (degree)	View angle (degree)
September 16th, 2022	0.00	0.07	146.87	42.44	2.97
September 17th, 2022	0.00	0.02	146.91	42.02	3.55
March 10th, 2023	0.06	0.19	146.10	34.70	3.72
March 11th, 2023	4.99	0.00	146.43	35.31	3.00
March 12th, 2023	0.03	0.21	144.85	35.18	2.62
March 15th, 2023	0.10	0.15	144.24	36.19	3.29

Table 1
Band configuration for the PSOA8BSR imagery.

Bands name	Coastal Blue	Blue	Green I	Green II	Yellow	Red	Red-Edge	NIR
Central Wavelength (nm)	443	490	531	565	610	665	705	865
Band Width (nm)	20	50	36	36	20	31	15	40

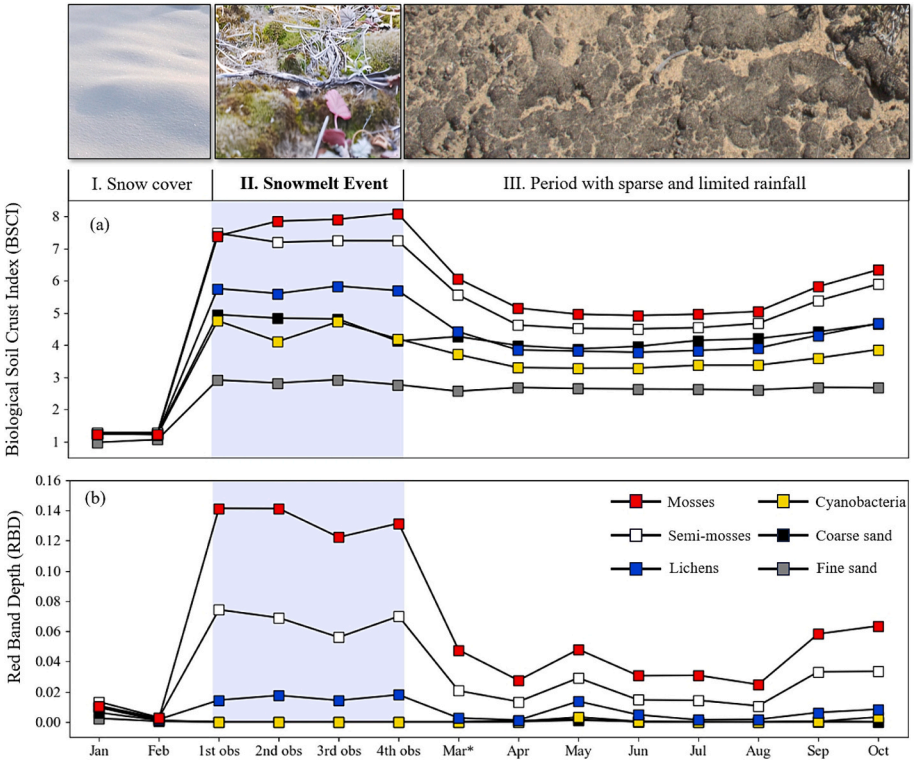

Fig. 4. Hydration-induced spectral response of biocrusts at different successional stages. I, II and III represent three typical periods in the Gurbantunggut Desert during the year. (a) and (b) represent the average BSCI and RBD series, respectively, from PSOA8BSR images across our sample plots (Section 2.2.1) in 2023. The observations labeled "month name" denote the monthly compositions, while those marked as "1st, 2nd, 3rd, and 4th" refer to the observations during the snowmelt period. Mar* refers to the ten-day composite from March 20 to 30.

Table 3
Definition of the biocrust succession categories.

Primary class	Secondary class	Definition	Reference
Biocrusts	cyanobacteria	lichens and mosses coverages <20%	Lan et al. (2013)
	lichens	lichens coverage >20% but mosses coverage <20%	
	semi-mosses	mosses coverage >20% but <75%	
	mosses	mosses coverage >75%	
Non-Biocrust	Coarse sand	0.63 mm < grain size <2 mm	ISO 14688-1:2017
	Fine sand	63 μm < grain size <0.63 mm	

where R_{green}, R_{red}, and R_{NIR} represent the reflectance of the green II, red and near-infrared bands, respectively. R^{mean}_{GRNIR} is the mean of the reflectance values across the green II, red and near-infrared bands. The adjustment parameter L is set to a value of 2, as recommended by Chen et al. (2005). $R^{envelope}_{Red}$ refers to the upper envelope value of the red band. CW_{green}, CW_{red} and CW_{NIR} denote the central wavelengths of the green II, red, and near-infrared bands, which are 565, 665 and 865 nm, respectively, in this study. Using the Gurbantunggut Desert as an example, Fig. 4 shows the changes in the BSCI and RBD during one year for biocrusts at different successional stages. The snowmelt event not only enhances the contrast between biocrusts and background (i.e., fine and coarse sand) but also aids in distinguishing among various stages of biocrust succession (i.e., cyanobacteria, lichens, semi-mosses and mosses). Furthermore, the spectral response signals remained stable during this period, making this event ideal for mapping biocrust succession.

Based on Eq.1 and Eq. 2, the BSCI and RBD were calculated for both the wet (the snowmelt period) and dry periods. After combining the two indices and the eight reflectance bands, two 10-band images for the wet and dry periods were generated by averaging the images for each period. In addition, a difference image (10 bands) was derived by subtracting the dry image from the wet image. In the following section, the spectral features from the wet, dry and difference images were prefixed with "wet", "dry" and "Δ", respectively. Finally, a 30-band feature image was created by concatenating these "wet", "dry" and "Δ" spectral features for the subsequent mapping procedure.

3.2. Two-stage random forest classification

The random forest (RF) model is an ensemble classifier that combines multiple decision trees generated from random subsets of training samples and features (Belgiu and Drăguţ, 2016). Its remarkable performance, interpretability, ease of implementation and high efficiency make it widely applied for various mapping tasks. Considering the sensitivity of RF to the proportion of samples in different classes (sample imbalance for classes) and the higher classification performance for the optimized features, this study employed a two-stage mapping framework (Hu et al., 2021; Sun et al., 2004) using the RF model based on different subsets of training samples and features (Fig. 5). In the first stage, RF was used to identify biocrusts against non-biocrust (fine and coarse sand), while in the second stage, RF was used to differentiate biocrusts at different successional stages, including cyanobacteria, lichens, semi-mosses, and mosses. Both biocrust and non-biocrust samples were used in Stage I mapping, whereas only biocrust samples were used in Stage II mapping. For each stage, the samples were partitioned into two spatially independent sets, in which 70% of the data were allocated to the training set and 30% to the test set. To reduce the computational burden induced by correlated and irrelevant features, a forward selection process was implemented for each stage to identify the most important features. This iterative process was initiated by training the

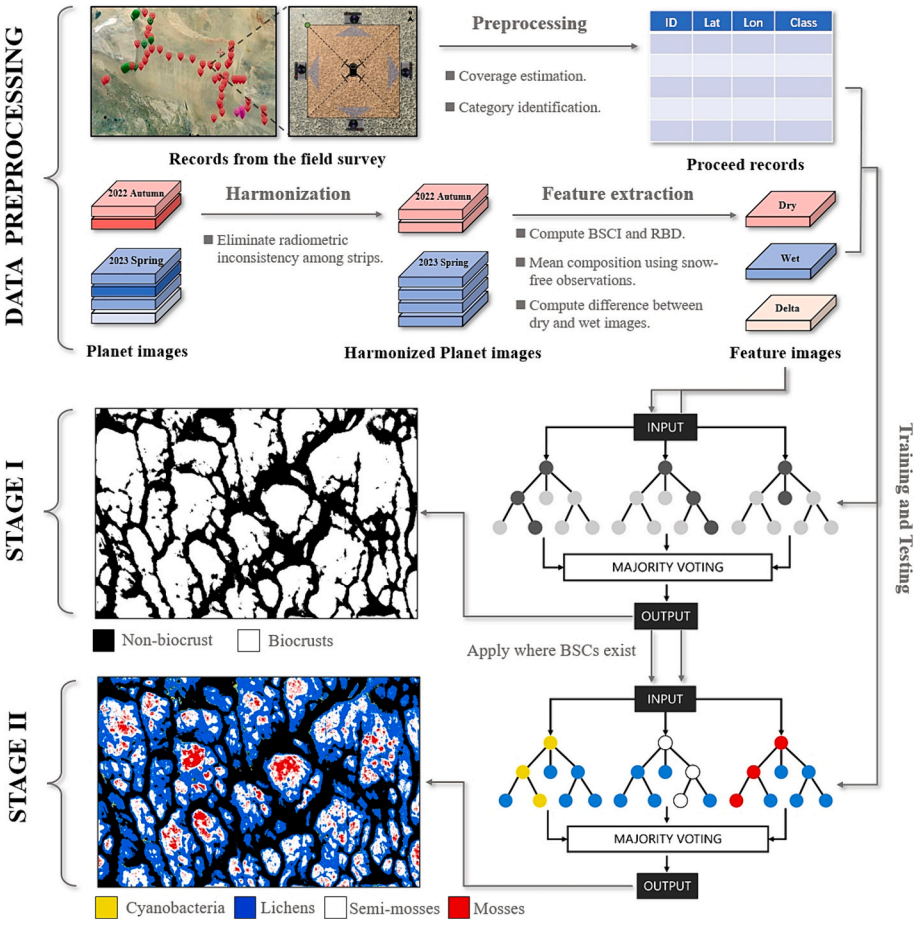

Fig. 5. Two-stage random forest classification.

RF classifier with a single feature that achieved the highest out-of-bag (OOB) accuracy. Subsequently, one feature at a time, which contributed the greatest improvement to the OOB accuracy during each training cycle, was added sequentially. The iteration stopped when the maximal OOB accuracy was reached. Once the essential features were identified, the RF model was trained using 500 trees and a maximum tree depth of 3. The performance of the RF classifier for each stage was evaluated using the precision (Eq. 4), recall (Eq. 5), and F1 score (Eq. 6) of the different categories.

$$Precision_i = \frac{TP_i}{TP_i + FP_i} \tag{4}$$

$$Recall_i = \frac{TP_i}{TP_i + FN_i} \tag{5}$$

$$F1\ score_i = 2 \times \frac{Precision_i \times Recall_i}{Precision_i + Recall_i} \tag{6}$$

TP, FP, and FN denote true positive (i.e., positive instances predicted correctly), false positive (i.e., positive instances predicted incorrectly) and false negative (i.e., negative instances predicted incorrectly) instances, respectively. The index "i" represents different categories, namely biocrusts, non-biocrusts (Stage I), cyanobacteria, lichens, semi-mosses and mosses (Stage II) in this study. After testing and finalizing the classifier, it was applied across the desert where snowmelt occurred and valid observations were available. Fig. 5 shows the flowchart of this study.

4. Results

4.1. Spectral responses of biocrusts at different successional stages to a hydration event (snowmelt)

Fig. 6 shows the spectra of biocrusts at different successional stages and fine and coarse sand under dry and wet conditions. Under dry conditions, it is possible to distinguish biocrusts (Fig. 6 (c)-(f)) from fine sand (Fig. 6(a)) since the latter has a much higher reflectance. Conversely, it is difficult to distinguish biocrusts from coarse sand (Fig. 6 (b)) because both types of cover have lower reflectance. However, upon hydration, the biocrusts exhibited a noticeable decrease in reflectance across all bands (Fig. 6(i)-(l)), while the coarse sand was essentially unresponsive (Fig. 6 (h)). This "darkening" effect facilitates the accurate identification of biocrusts. On the other hand, these changes in reflectance are similar for biocrusts of different successional stages and thus insufficient to distinguish successional stages. Fortunately, late successional biocrusts (i.e., semi-mosses and mosses) exhibit varying degrees of red-light absorption due to photosystem reactivation (Fig. 6(q) and (r)), in contrast to early successional biocrusts that lack such a response (Fig. 6(o) and (p)). This finding aligns with that of Rieser et al., who also observed an increase in photosynthetic intensity proxy of biocrusts (NDVI) following hydration events (Rieser et al., 2021). This "greening" effect helps to distinguish between biocrusts at different successional stages.

Two spectral indices, the BSCI and RBD, were used in this study to quantify the aforementioned "darkening" and "greening" effects. Fig. 7 illustrates the changes in these parameters between dry and wet conditions. Biocrusts consistently exhibited clear increases in BSCI regardless of successional stage, whereas no such changes were observed in

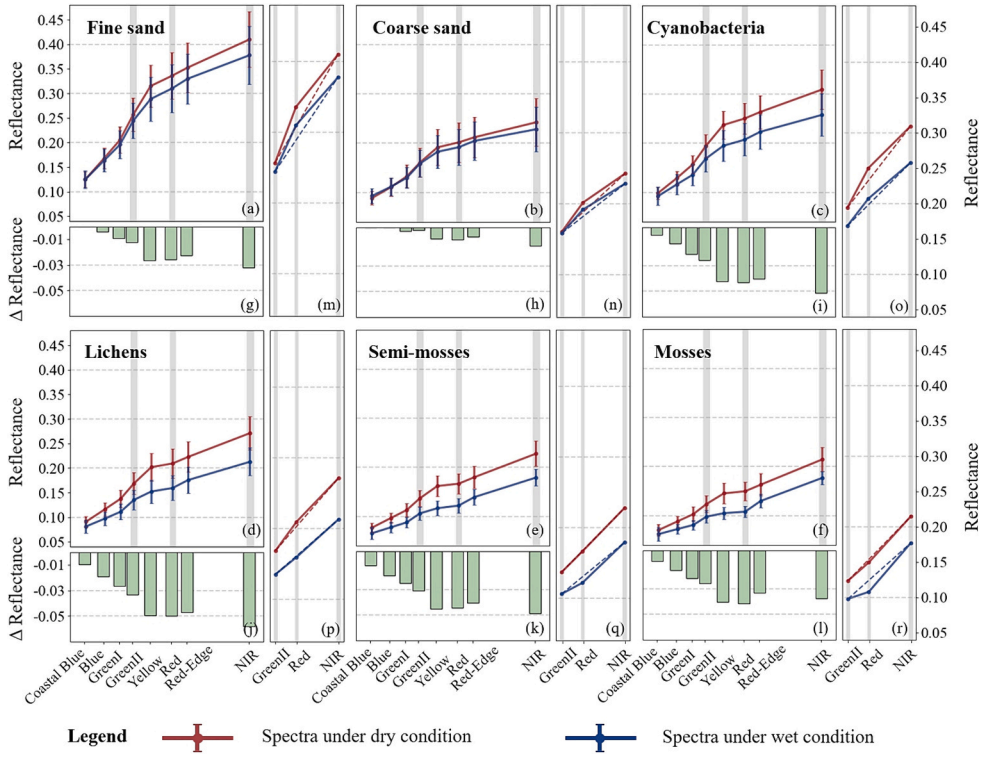

Fig. 6. Spectral changes in biocrusts at various successional stages and fine and coarse sand under dry and wet conditions. (a) – (f) Spectra under dry (red) and wet (blue) conditions. (g) – (l) Differences in spectra between two conditions (wet spectra minus dry spectra). (m) – (r) Red band absorption under both conditions, with the dashed line representing the upper envelope from the Green II to NIR region. The location of Green II, Red and NIR bands are marked in translucent gray bars. A greater deviation of the red band reflectance below the envelope (dashed line) indicates a more pronounced absorption feature. The data were acquired from the PSOA8BSR images of our sample plots (Section 2.2.1). (For interpretation of the references to colour in this figure legend, the reader is referred to the web version of this article.)

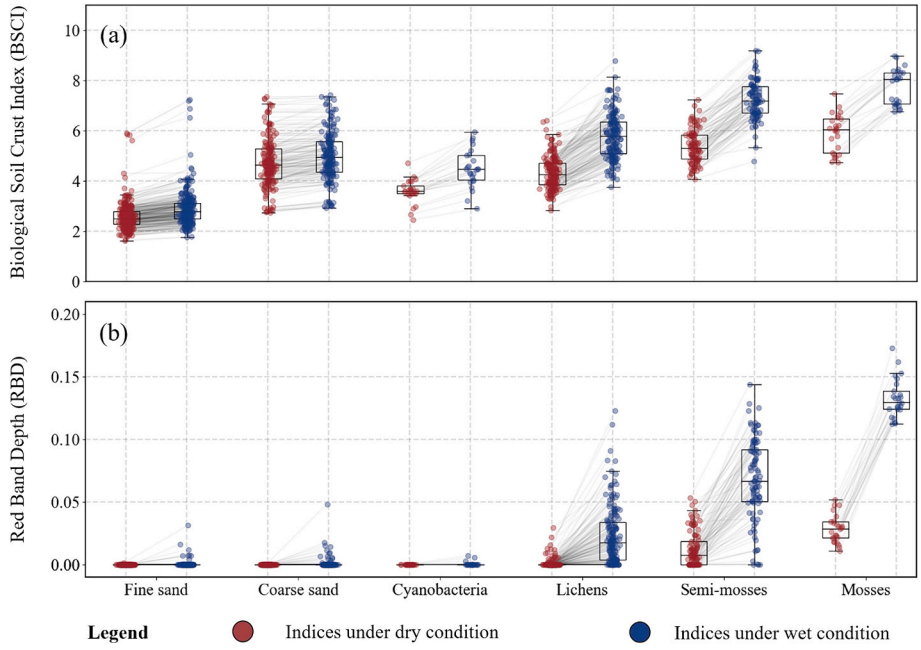

Fig. 7. (a) Biological Soil Crust Index (BSCI) and (b) Red Band Depth (RBD) of biocrusts at different successional stages and fine and coarse sand under dry and wet conditions. The median lines are shown in black for each boxplot, and the corresponding sample points under both conditions are connected by light gray lines. The data were acquired from the PSOA8BSR images of our sample plots (Section 2.2.1). (For interpretation of the references to colour in this figure legend, the reader is referred to the web version of this article.)

either fine or coarse sand (Fig. 7(a)). Furthermore, late-stage biocrusts clearly exhibited red-light absorption (evident as a decrease in the RBD), whereas weaker or no such responses were observed in early-stage biocrusts (Fig. 7 (b)). Notably, some lichen samples exhibited red-light absorption, albeit weakly, consistent with the findings of Phinney et al. (2018). In summary, a hydration event (snowmelt) not only enhances the contrast between biocrusts and their background (i.e., fine and coarse sand) through the "darkening" effect but also helps to distinguish between different stages of biocrust succession (i.e., cyanobacteria, lichens, semi-mosses, and mosses) through the "greening" effect. These features show great potential for biocrust succession mapping.

Fig. 8 shows the spatial patterns of the BSCI and RBD based on PlanetScope images in the desert under dry and wet conditions. On a regional scale, the BSCI in the southwestern (A), central (B), southeastern (C), and eastern (D) areas significantly increased after hydration (Fig. 8(a)-(c)), indicating the prevalence of biocrusts in these areas. However, the eastern (D) area (Fig. 8(e) and (f)) showed no change in the RBD, suggesting the dominance of early-stage biocrusts such as cyanobacteria and lichens. Conversely, significant changes in the RBD were observed in the remaining areas and were particularly intense in the southwestern area (A), indicating the widespread presence of late stage biocrusts such as semi-mosses and mosses. On a landscape scale, biocrusts showed a clear increase in BSCI after hydration compared to non-biocrust areas (Fig. 8(g)-(l)). In addition, higher RBD responses were found in the central interdune area (Fig. 8(o) and (q)), suggesting a distribution of late-stage biocrusts in this area. These results highlight the potential of BSCI and RBD images to map the spatial distribution of biocrust succession at multiple scales, from landscape to regional.

4.2. *Biocrust succession mapping based on two-stage random forest classification*

Tables 4 and 5 show the performance metrics for each mapping stage. The framework achieved promising overall accuracies of 0.958 and 0.802 for Stage I and Stage II, respectively. It accurately identified biocrusts from both fine and coarse sand, demonstrating high precision (0.963) and recall (0.951). For mapping the biocrust succession stages, the framework achieved notable F1-*scores*: 0.828 for mosses, 0.741 for semi-mosses, 0.857 for lichens, and 0.588 for cyanobacteria. All the samples used for the test were collected during the field survey mentioned in Section 2.2.1. Notably, there were no misclassifications between nonadjacent stages, such as lichens and mosses, but a few occurred between adjacent stages, such as lichens and semi-mosses or semi-mosses and mosses. This is due to the gradual nature of biocrust succession, which results in similarities in spectral features between adjacent stages. However, the framework encounters challenges in identifying cyanobacteria, primarily because their light colour can be mistaken for that of certain light-colored lichens (Rodríguez-Caballero et al., 2014). Nevertheless, the proposed framework shows effectiveness in both biocrust identification and biocrust succession mapping.

Fig. 9 shows the biocrust succession mapping results. Six representative areas across the desert (Fig. 9(a)–(e)) are magnified for detail. At the regional scale, cyanobacteria and lichens dominate expansive areas, while semi-mosses are abundant in the central (Fig. 9(b-1) and (b-2)) and southeastern (Fig. 9(e-1) and (e-2)) regions of the desert. Notably, the southwestern (Fig. 9(d-1) and (d-2)) part of the desert exhibits a prevalence of mosses, an aspect often overlooked previously. Conversely, early-stage biocrusts were predominantly distributed in the northwestern regions (Fig. 9 (c-1) and (c-2)). In addition, biocrusts rarely occur on either the western or eastern side of the desert because

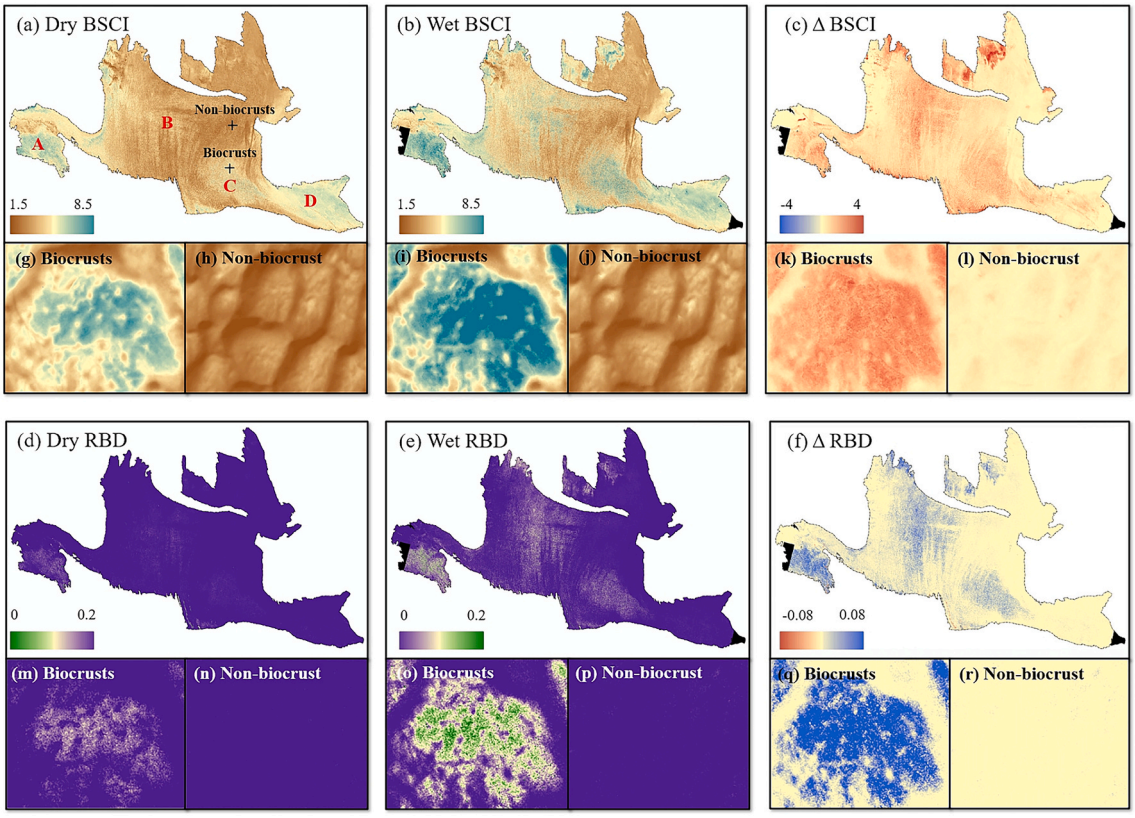

Fig. 8. (a) – (f) The spatial patterns of the Biological Soil Crust Index (BSCI) and Red Band Depth (RBD) in the Gurbantunggut Desert under dry and wet conditions and their differences between the two conditions. (g) – (r) Index images of two typical areas: biocrusts and non-biocrusts (marked by crosses in (a)). Locations A to D in (a) serve as representative areas to illustrate spatial patterns. All the index images are derived from the PSOA8BSR images.

Table 4
Performance evaluation of Stage I classification.

Stage-I	Samples for non-biocrust	Samples for biocrusts	Precision	Recall	F1-*score*	Overall Accuracy
Non-biocrust	**156**	2	0.945	0.987	0.966	–
Biocrusts	9	**96**	0.980	0.914	0.946	–
Mean (macro)	–	–	0.963	0.951	0.956	0.958

Table 5
Performance evaluation of Stage II classification.

Stage-II	Samples for Cyanobacteria	Samples for Lichens	Samples for Semi-mosses	Samples for Mosses	Precision	Recall	F1-*score*	Overall Accuracy
Cyanobacteria	**5**	2	0	0	0.500	0.714	0.588	–
Lichens	5	**48**	1	0	0.828	0.889	0.857	–
Semi-mosses	0	8	**20**	2	0.833	0.667	0.741	–
Mosses	0	0	3	**12**	0.857	0.800	0.828	–
Mean (macro)	–	–	–	–	0.754	0.767	0.753	0.802

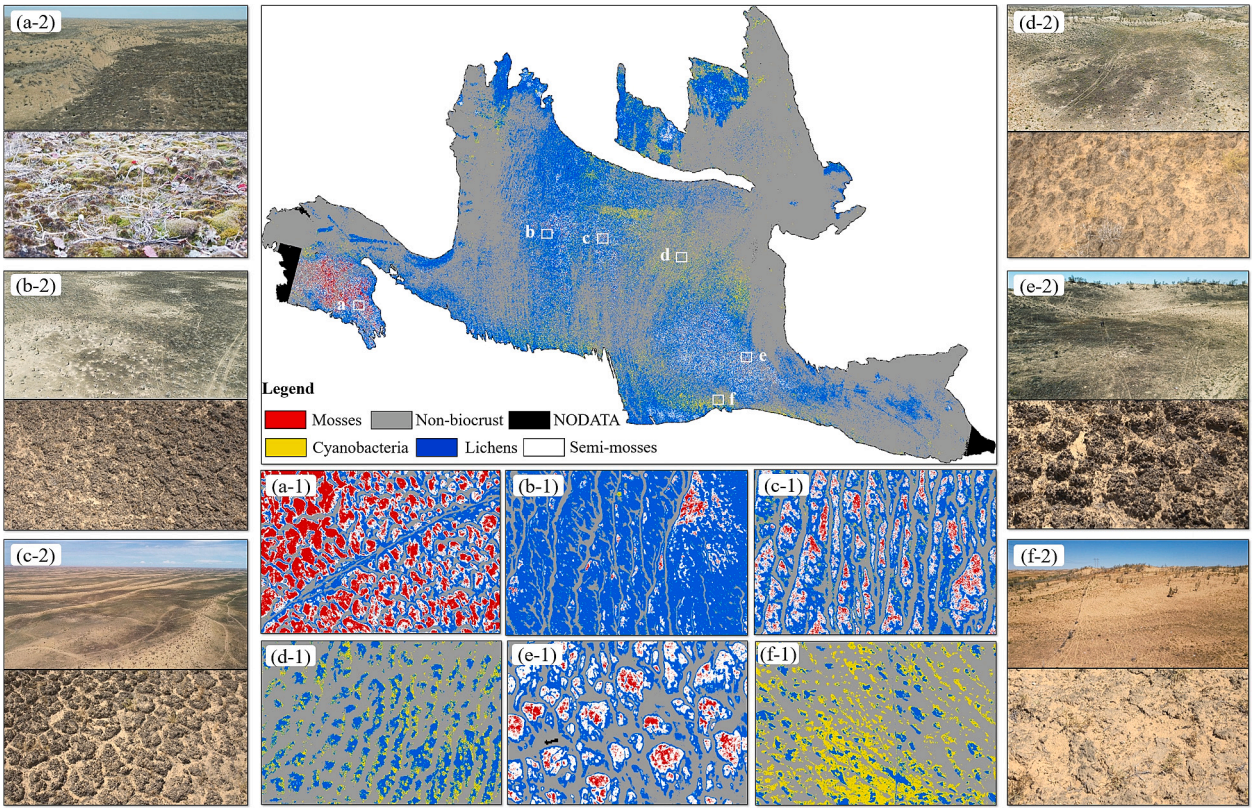

Fig. 9. Mapping of biocrust succession across the Gurbantunggut Desert. Panels (a-1) through (f-1) show detailed maps of six representative regions across the desert. Panels (a-2) through (f-2) show in situ images of these regions.

these areas are largely covered by coarse sand. At the landscape scale, late-stage biocrusts were observed in the interdune zones, while early-stage biocrusts occurred on the slopes of the sand dunes, consistent with previous field observations (Zhang et al., 2010).

4.3. Feature importance by the forward feature selection

Fig. 10(a) and (b) depict the out-of-bag (OOB) accuracy curves for forward feature selection in Stage I and Stage II mapping, respectively. The curves reveal an initial increase in accuracy, reaching a peak, followed by a gradual decrease, implying that crucial information is integrated in the early stages of feature selection, with subsequent stages potentially incorporating redundant or irrelevant information. Therefore, the feature subset that achieved the maximum OOB accuracy was used to finalize the classification model. Fig. 10(c) and (d) illustrate the initial eight feature selection processes, where the candidate features are ranked based on their contribution to OOB accuracy improvement at each step. Notably, hydration-induced features (i.e., prefixed as "wet" or "Δ") outweigh ordinary features (i.e., prefixed as "dry"), constituting 85% and 100%, respectively, of the final feature subset for each of the two mapping stages (i.e., highlighted in yellow). Specifically, Stage I mapping achieved an OOB accuracy of 0.947 solely based on the Δ BSCI, while for Stage II, only the wet RBD and wet Green II band were needed to reach the maximum OOB accuracy (0.812). This result consistent with Román et al.'s findings, which establish the red band absorption feature as a reliable indicator of biocrust photosynthetic intensity due to its strong correlation with Chlorophyll *a* content (Román et al., 2019).

Fig. 11 shows scatter plots of the two most important features for Stage I (i.e., Δ BSCI vs. Δ Blue) and Stage II (i.e., Wet RBD vs. Wet Green II band) mapping, along with the decision boundaries for each stage. As

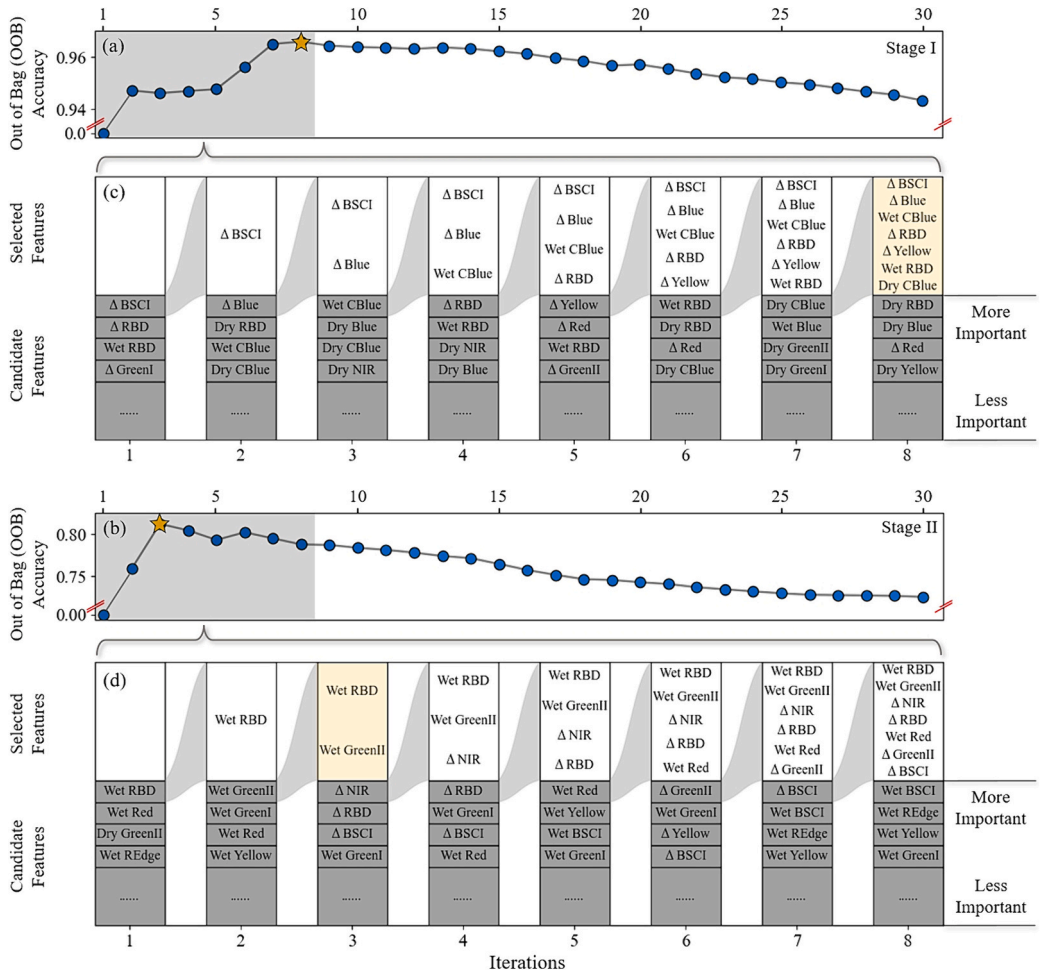

Fig. 10. Feature importance by the forward feature selection. Panels (a) and (b) show the out-of-bag (OOB) accuracy curves for Stage I and II mapping, respectively, with asterisks indicating maximum accuracy. Panels (c) and (d) detail the initial eight steps of the iterative feature selection process. For each step, the feature with the highest relative importance is positioned at the top and selected for the subsequent iteration. The feature subsets used in the final classification models are highlighted in yellow. (For interpretation of the references to colour in this figure legend, the reader is referred to the web version of this article.)

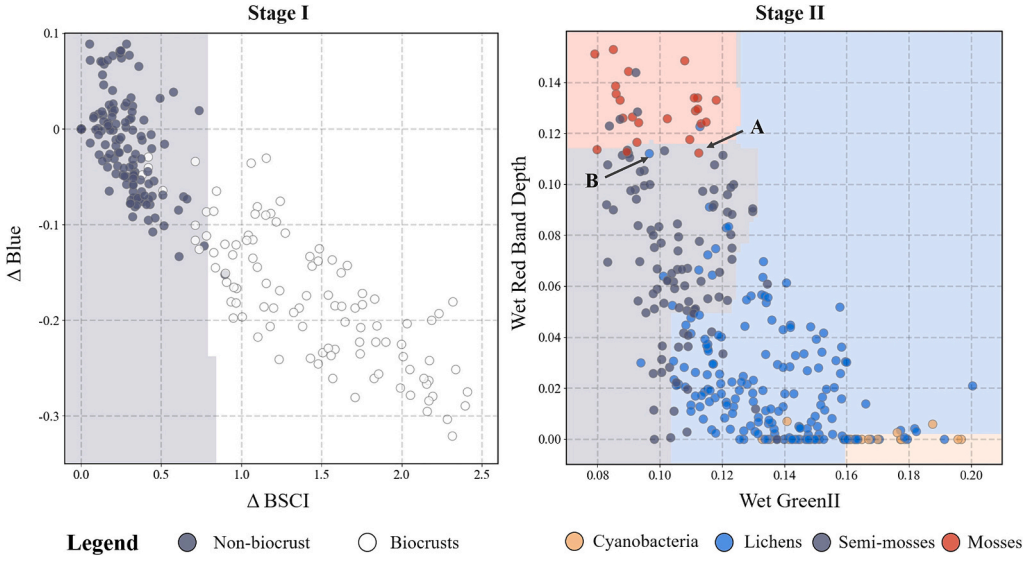

Fig. 11. Analysis of the two most important features at each stage of biocrust succession mapping. The decision boundaries of the classification model (RF) for each stage are set as background. Points A and B represent two anomalies encountered during the mapping process.

depicted in Fig. 11(a), biocrusts exhibit a greater increase in BSCI after hydration than non-biocrust due to their superior water retention. Fig. 11(b) shows that due to the inherent differences among the different successional biocrusts, late-stage biocrusts not only exhibited lower reflectance in the Green II band after hydration but also exhibited greater photosynthetic intensity (Wet RBD). However, there are exceptions; for example, moss site A has a weaker photosynthetic intensity due to the threat of sand burial, while lichen site B has a greater photosynthetic intensity due to favorable growing conditions and the coexistence of mosses. Nevertheless, forward selection ensures that essential features are included while avoiding noise from irrelevant features. More importantly, the selected features highlighted the importance of hydration-induced spectral features for both stages of biocrust succession mapping.

5. Discussion

5.1. Necessity of biocrust succession mapping

Biocrusts at different successional stages have diverse ecological functions and interact differently with abiotic and biotic components. Mapping this succession holds great potential for enhancing our understanding of desert ecosystem dynamics, including their structure, ecological services, and responses to climate change and human intervention. There are at least three critical research areas where mapping biocrust succession can contribute: First, different successional biocrusts have distinct effects on soil physicochemical (e.g., soil structure, pH and salinity) and biological (e.g., microbial respiration, protein content and total chlorophyll) properties (Atashpaz et al., 2023; Chamizo et al., 2012a; Concostrina-Zubiri et al., 2013). They also play various roles in carbon and nitrogen cycling (Housman et al., 2006; Lan et al., 2021; Tian et al., 2023; Wu et al., 2023). Moreover, late-stage biocrusts notably enhance soil aggregate stability and water retention compared to early-stage biocrusts, thereby improving resistance against wind and water erosion (Drahorad et al., 2021; Gall et al., 2022; Lázaro et al., 2023; Yang et al., 2022). Therefore, mapping these stages can help elucidate their roles in regional environmental modeling. For instance, 35.08% of the Gurbantunggut Desert was covered by biocrusts, with lichens accounting for the largest proportion at 76.68%, followed by cyanobacteria and semi-mosses at 11.24% and 9.81%, respectively. Mosses made up the smallest proportion with only 2.26%. Combined with field survey data on carbon and nitrogen fixation rates and wind and water repellency, these proportion data allow quantification of their respective contributions to carbon and nitrogen pools and their distinct effects on regional aeolian and hydrologic systems. Second, late-stage biocrusts, such as mosses and lichens, are highly susceptible to physical disturbance and climate-induced stress (Phillips et al., 2022) and require decades to recover (Deng et al., 2020). In this context, the successional stages of biocrusts serve as valuable bioindicators of dryland ecosystem change (Belnap et al., 2013; Chamizo et al., 2012b; Holt and Miller, 2010), and can provide guidance for prioritizing conservation strategies. For instance, early-stage biocrusts are predominantly found in northeastern desert regions, while late-stage biocrusts are more common in the southeastern, central, and southwestern deserts. This distribution pattern can be used as a guide to prioritize conservation areas (e.g., late-stage biocrust distribution areas). In addition, by obtaining biocrust succession maps over multiple years, researchers can assess disturbance or stress levels, allowing for timely protection of affected biocrusts. Third, biocrust succession mapping highlights their spatial distribution, facilitating field survey planning. By integrating the mapping results with multiple Geographic Information Systems (GIS) data layers, such as road vectors, researchers can efficiently sample different successional biocrusts from different habitats.

5.2. Event-induced spectral features vs. multi-temporal spectral features

In general, multi-temporal images provide comprehensive spectral information about land surface changes, leading to promising mapping performance in most applications. However, this is not always the case. Short-term spectral responses induced by specific events not only capture specific spectral features that are generally difficult to observe, but also reduce the need for multi-temporal imagery, thereby reducing data acquisition and processing costs. Fig. 12 compares the effectiveness of hydration-induced and multi-temporal (i.e., April to October) spectral features for mapping biocrust succession. Hydration-induced features comprise 8-band spectral reflectance and 2 indices under dry and wet conditions, along with their differences (30 in total). The multi-temporal features comprise monthly compositions of 8-band spectral reflectance and 2 indices from April to October (70 in total). The monthly averaging composition mitigates cloud cover and cross-sensor radiometric inconsistencies. Independent forward selection procedures (as described in 4.3) were performed for both hydration-induced (i.e., blue dots) and multi-temporal (i.e., red dots) feature sets for Stage I (Fig. 12(a)) and Stage II (Fig. 12(c)) mapping. The OOB accuracy is consistently greater for hydration-induced features than for multi-temporal features. For Stage I mapping, 7 hydration-induced features achieve a maximum OOB accuracy of 0.966, while 19 multi-temporal features achieve a maximum accuracy of 0.942. For Stage II, 2 hydration induced features achieve a maximum OOB accuracy of 0.812, whereas 5 multi-temporal features achieve a maximum accuracy of 0.756. The feature subsets with the maximum OOB accuracy were subsequently used to finalize the classification model. The model using hydration-induced features outperforms that using multi-temporal features in both stages (Fig. 12(b) and (d)). Especially in stage II, hydration-induced features showed significantly greater effectiveness (F1 score = 0.75) compared to multi-temporal features (F1 score = 0.43). This finding suggested that although multi-temporal features provide more spectral information, they are less effective than hydration-induced features in mapping biocrust succession. These results imply that the use of a few essential event-induced features may outperform the use of multi-temporal but irrelevant features.

5.3. Biocrust succession mapping based on rainfall-induced spectral response signals

This study demonstrated the effectiveness of using distinct spectral responses to snowmelt events for mapping biocrusts at different successional stages. However, such snowmelt events do not always occur in other deserts around the world, especially in hot deserts characterized by infrequent hydration events (only infrequent rainfall events). It is reasonable to ask whether it is possible to use rainfall events instead of snowmelt events to map successional biocrusts. The answer to this question could ensure that the methodology proposed in this study can be applied to other deserts around the world where rainfall events are a common occurrence. Previous studies have shown that a rainfall-induced spectral response similar to that induced by snowmelt can be observed in numerous desert ecosystems with widespread biocrust distribution, including the Negev Desert in Israel, the Mu Us Sandy Land in China, and the Colorado Plateau in the United States (Chen et al., 2023). Thus, the proposed method has potential as a roadmap for global biocrust succession mapping if spectral responses triggered by rainfall pulses can be observed. To further investigate this possibility, two representative areas dominated by early-stage (i.e., cyanobacteria and lichens) and late-stage (i.e., semi-mosses and mosses) biocrusts were selected in the Gurbantunggut Desert for rainfall-induced mapping tasks. Here, testing is still confined to this desert, as we could not conduct intensive field surveys in other deserts. Both areas experienced significant rainfall from July 30 to 31, 2021. Therefore, PSOA8BSR images on July 29 and August 1, 2021, were employed as dry and wet images, respectively. All relevant feature images were prepared, as

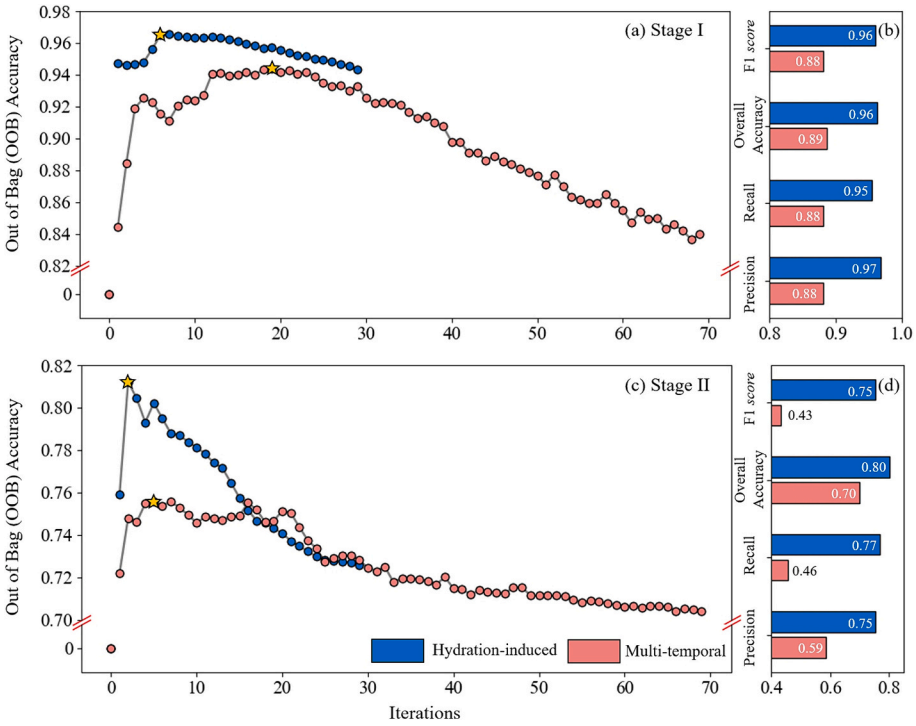

Fig. 12. Comparison between hydration-induced and multi-temporal spectral features regarding their effectiveness in biocrust succession mapping. (a) and (c) show the changes in OOB accuracy in the forward selection procedure for Stages I and II, respectively. There are 30 hydration-induced features (i.e., blue dots) and 70 multi-temporal features (i.e., red dots) awaiting the selection procedure. The feature set that achieved the highest OOB accuracy was used to finalize the model. (b) and (d) Performance of the finalized model for Stages I and II, respectively. (For interpretation of the references to colour in this figure legend, the reader is referred to the web version of this article.)

outlined in Section 3.1. Using the ground-truth samples collected during the 2023 field survey (there was very little change between 2021 and 2023), random forest models were separately trained for each area using only the most important features, as detailed in the Section 4.3. Fig. 13 illustrates a comparison of biocrust succession mapping using rainfall and snowmelt induced spectral responses. In both selected areas, two types of hydration events induced significant but similar changes in the Biological Soil Crust Index (BSCI) and Red Band Depth (RBD) values (Fig. 13 (a) - (l)). Consequently, biocrust succession mapping using rainfall-induced spectral responses exhibited only minor differences compared to using snowmelt-induced spectral responses (Fig. 13 (m) – (p)), suggesting that the spectral responses triggered by rainfall events has potential to be applied to other deserts if rainfall events exist. However, it is important to acknowledge that desert rainfalls are generally localized and heterogeneous, resulting in different spectral response intensities at different locations. Accordingly, the mapping of the biocrust succession should be carried out for each sub-area using different local rainfall events and then be merged together to cover large areas. Given that current mainstream meteorological products provide precipitation records with global coverage at an hourly resolution, identifying local rainfall events within potential biocrust distribution areas has become an increasingly straightforward task.

6. Conclusions

Biocrusts at different successional stages have different ecological functions and serve as important bioindicators of changes in desert ecosystems. Few attempts have been made to map biocrusts at different successional stages. As a pioneering study, this study takes full advantage of the diverse spectral responses of biocrusts at different successional stages to hydration events, i.e., late-stage biocrusts exhibit lower reflectance (i.e., darkening effect) and increased red light absorption (i.e., greening effect) upon hydration due to their superior water retention and photosystem recovery. Based on the spectral response induced by snowmelt events, this study proposes a two-stage classification framework for mapping biocrust succession and applies it to the Gurbantunggut Desert. The results showed that snowmelt induces noticeable changes in biocrust spectra, facilitating differentiation between biocrusts and other components or between different stages of biocrust succession. The mapping framework achieved overall accuracies of 0.958 and 0.802 for Stage I and Stage II, respectively, highlighting its ability to delineate spatial patterns of successional stages across landscape and regional scales. At the regional scale, cyanobacteria and lichens dominate expansive areas, while semi-mosses are abundant in the central and southeastern regions of the desert. Notably, the southwestern part of the desert contains a prevalence of mosses, which has not been found in previous studies. At the landscape scale, late-stage biocrusts were observed in the interdunes, while early-stage biocrusts occurred on the slopes of the sand dunes, consistent with field observations. This study lays the groundwork for future in-depth investigations of desert ecosystem dynamics, including structure, ecological services, and responses to climate change and human activities. Furthermore, event-induced spectral features may have great potential for application in classification tasks, as they not only capture specific spectral features that are generally difficult to observe but also reduce the cost of acquiring and processing multi-temporal image data.

CRediT authorship contribution statement

Ruilin Chen: Writing – original draft, Visualization, Validation, Methodology, Investigation, Formal analysis, Data curation, Conceptualization. **Benfeng Yin:** Writing – review & editing, Validation, Investigation, Funding acquisition, Formal analysis, Conceptualization. **Wei Yang:** Writing – review & editing, Funding acquisition. **Jianlong Li:** Writing – review & editing, Investigation, Data curation. **Zeteng Li:** Writing – review & editing, Investigation, Data curation. **Yuanming**

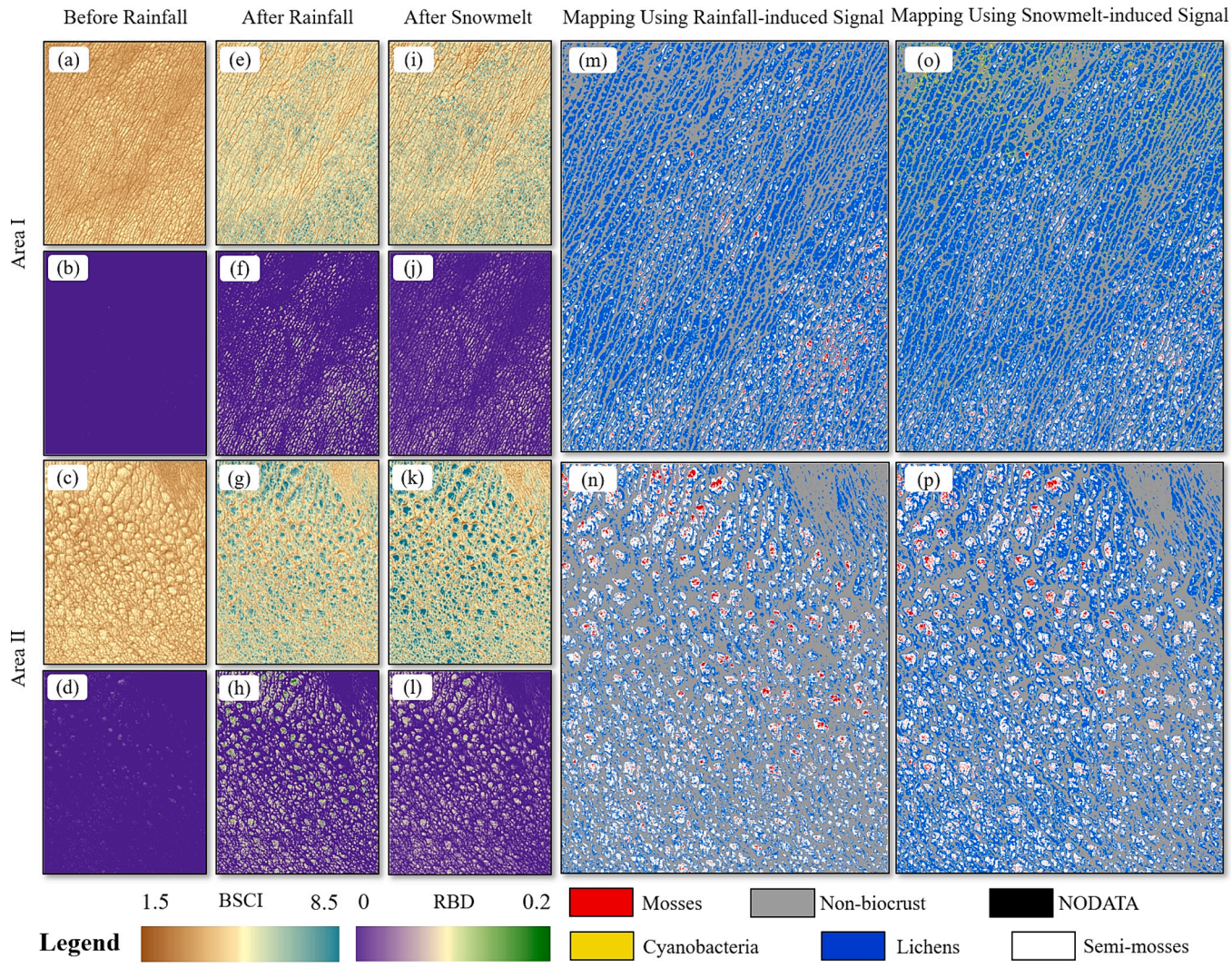

Fig. 13. Comparison of biocrust succession mapping using rainfall and snowmelt induced spectral responses. Two representative areas, Area I (i.e., dominated by early-stage biocrusts: cyanobacteria and lichens) and Area II (i.e., dominated by late-stage biocrusts: semi-mosses and mosses), were selected. Both areas received substantial rainfall (13.2 mm and 20.5 mm, respectively, from ECMWF data) from July 30 to 31, 2021. PSOA8BSR images on July 29 and August 1, 2021 was used as dry and wet images for mapping. (a) – (d) Biological Soil Crust Index (BSCI) and Red Band Depth (RBD) images before rainfall, (e) – (h) after rainfall and (i) – (l) after snowmelt. (m) – (n) Biocrust succession mapping results based on rainfall-induced spectral response signals. (o) – (p) Mapping results based on snowmelt-induced signals. (For interpretation of the references to colour in this figure legend, the reader is referred to the web version of this article.)

Zhang: Writing – review & editing, Supervision, Conceptualization. **Jin Chen:** Writing – review & editing, Supervision, Methodology, Investigation, Funding acquisition, Conceptualization.

Declaration of competing interest

The authors declare no potential conflicts of interest with respect to the research, authorship, or publication of this article.

Data availability

The authors do not have permission to share data.

Acknowledgments

This study was supported by National Natural Science Foundation of China [grant Number U2003214]; the Japan Society for the Promotion of Science (JSPS) KAKENHI [grant Number 23K18517] and the Virtual Laboratory (VL) project supported by the Ministry of Education, Culture, Sports, Science and Technology (MEXT), Japan; and the Youth Innovation Promotion Association of the Chinese Academy of Sciences [grant Number 2020437]. The authors would like to express their sincere gratitude to the three anonymous reviewers and the editor for their invaluable suggestions and insightful comments, which have greatly improved the quality of our manuscript. The authors would also like to thank Mr. Dian Fu Ren for bringing the authors safely into and out of the desert.

Appendix A. Supplementary data

Supplementary data to this article can be found online at https://doi.org/10.1016/j.rse.2024.114230.

References

Atashpaz, B., Khormali, F., Malekzadeh, E., Soleymanzadeh, M., 2023. Evaluating the effect of different sequences of biological crusts on loess derived soil biophysiological properties in the semi-arid regions of Northern Iran. J. Soil Sci. Plant Nutr. 23, 6777–6787. https://doi.org/10.1007/s42729-023-01535-6.

Beaugendre, N., Malam Issa, O., Choné, A., Cerdan, O., Desprats, J.-F., Rajot, J.L., Sannier, C., Valentin, C., 2017. Developing a predictive environment-based model

for mapping biological soil crust patterns at the local scale in the Sahel. CATENA 158, 250–265. https://doi.org/10.1016/j.catena.2017.06.010.
Belgiu, M., Drăguţ, L., 2016. Random forest in remote sensing: a review of applications and future directions. ISPRS J. Photogramm. Remote Sens. 114, 24–31. https://doi.org/10.1016/j.isprsjprs.2016.01.011.
Belnap, J., Gillette, D.A., 1998. Vulnerability of desert biological soil crusts to wind erosion: the influences of crust development, soil texture, and disturbance. J. Arid Environ. 39, 133–142. https://doi.org/10.1006/jare.1998.0388.
Belnap, J., Phillips, S.L., Witwicki, D.L., Miller, M.E., 2008. Visually assessing the level of development and soil surface stability of cyanobacterially dominated biological soil crusts. J. Arid Environ. 72, 1257–1264. https://doi.org/10.1016/j.jaridenv.2008.02.019.
Belnap, J., Wilcox, B.P., Van Scoyoc, M.W., Phillips, S.L., 2013. Successional stage of biological soil crusts: an accurate indicator of ecohydrological condition. Ecohydrology 6, 474–482. https://doi.org/10.1002/eco.1281.
Belnap, J., Walker, B.J., Munson, S.M., Gill, R.A., 2014. Controls on sediment production in two U.S. deserts. Aeolian Res. 14, 15–24. https://doi.org/10.1016/j.aeolia.2014.03.007.
Belnap, J., Weber, B., Büdel, B., 2016. Biological soil crusts as an organizing principle in drylands. In: Weber, B., Büdel, B., Belnap, J. (Eds.), Biological Soil Crusts: An Organizing Principle in Drylands. Springer International Publishing, Cham, pp. 3–13.
Bowker, M.A., Belnap, J., Miller, M.E., 2006. Spatial modeling of biological soil crusts to support rangeland assessment and monitoring. Rangel. Ecol. Manage. 59, 519–529. https://doi.org/10.2111/05-179r1.1.
Bowker, M.A., Doherty, K.D., Antoninka, A.J., Ramsey, P.W., DuPre, M.E., Durham, R.A., 2022. Biocrusts influence vascular plant community development, promoting native plant dominance. Front. Ecol. Evol. 10, 840324 https://doi.org/10.3389/fevo.2022.840324.
Bu, C.F., Zhang, P., Wang, C., Yang, Y.S., Shao, H.B., Wu, S.F., 2016. Spatial distribution of biological soil crusts on the slope of the Chinese Loess Plateau based on canonical correspondence analysis. CATENA 137, 373–381. https://doi.org/10.1016/j.catena.2015.10.016.
Chamizo, S., Cantón, Y., Miralles, I., Domingo, F., 2012a. Biological soil crust development affects physicochemical characteristics of soil surface in semiarid ecosystems. Soil Biol. Biochem. 49, 96–105. https://doi.org/10.1016/j.soilbio.2012.02.017.
Chamizo, S., Stevens, A., Cantón, Y., Miralles, I., Domingo, F., Van Wesemael, B., 2012b. Discriminating soil crust type, development stage and degree of disturbance in semiarid environments from their spectral characteristics. Eur. J. Soil Sci. 63, 42–53. https://doi.org/10.1111/j.1365-2389.2011.01406.x.
Chen, J., Yuan Zhang, M., Wang, L., Shimazaki, H., Tamura, M., 2005. A new index for mapping lichen-dominated biological soil crusts in desert areas. Remote Sens. Environ. 96, 165–175. https://doi.org/10.1016/j.rse.2005.02.011.
Chen, R., Tan, X., Zhang, Y., Chen, H., Yin, B., Zhu, X., Chen, J., 2023. Monitoring rainfall events in desert areas using the spectral response of biological soil crusts to hydration: evidence from the Gurbantunggut Desert, China. Remote Sens. Environ. 286, 113448 https://doi.org/10.1016/j.rse.2022.113448.
Colica, G., Li, H., Rossi, F., Li, D., Liu, Y., De Philippis, R., 2014. Microbial secreted exopolysaccharides affect the hydrological behavior of induced biological soil crusts in desert sandy soils. Soil Biol. Biochem. 68, 62–70. https://doi.org/10.1016/j.soilbio.2013.09.017.
Collier, E.A., Perroy, R.L., Reed, S.C., Price, J.P., 2022. Mapping biological soil crusts in a Hawaiian dryland. Int. J. Remote Sens. 43, 484–509. https://doi.org/10.1080/01431161.2021.2003904.
Concostrina-Zubiri, L., Huber-Sannwald, E., Martínez, I., Flores Flores, J.L., Escudero, A., 2013. Biological soil crusts greatly contribute to small-scale soil heterogeneity along a grazing gradient. Soil Biol. Biochem. 64, 28–36. https://doi.org/10.1016/j.soilbio.2013.03.029.
Deng, S., Zhang, D., Wang, G., Zhou, X., Ye, C., Fu, T., Ke, T., Zhang, Y., Liu, Y., Chen, L., 2020. Biological soil crust succession in deserts through a 59-year-long case study in China: how induced biological soil crust strategy accelerates desertification reversal from decades to years. Soil Biol. Biochem. 141, 107665 https://doi.org/10.1016/j.soilbio.2019.107665.
Drahorad, S.L., Felde, V.J.M.N.L., Ellerbrock, R.H., Henss, A., 2021. Water repellency decreases with increasing carbonate content and pH for different biocrust types on sand dunes. J. Hydrol. Hydromech. 69, 369–377. https://doi.org/10.2478/johh-2021-0022.
Eldridge, D.J., Leys, J.F., 2003. Exploring some relationships between biological soil crusts, soil aggregation and wind erosion. J. Arid Environ. 53, 457–466. https://doi.org/10.1006/jare.2002.1068.
Escolar, C., Martínez, I., Bowker, M.A., Maestre, F.T., 2012. Warming reduces the growth and diversity of biological soil crusts in a semi-arid environment: implications for ecosystem structure and functioning. Philos. Trans. R. Soc. Lond. B Biol. Sci. 367, 3087–3099. https://doi.org/10.1098/rstb.2011.0344.
Ferrenberg, S., Reed, S.C., Belnap, J., 2015. Climate change and physical disturbance cause similar community shifts in biological soil crusts. Proc. Natl. Acad. Sci. U. S. A. 112, 12116–12121. https://doi.org/10.1073/pnas.1509150112.
Frazier, A.E., Hemingway, B.L., 2021. A technical review of planet smallsat data: practical considerations for processing and using planetscope imagery. Remote Sens. (Basel) 13, 3930. https://doi.org/10.3390/rs13193930.
Gall, C., Nebel, M., Quandt, D., Scholten, T., Seitz, S., 2022. Pioneer biocrust communities prevent soil erosion in temperate forests after disturbances. Biogeosciences 19, 3225–3245. https://doi.org/10.5194/bg-19-3225-2022.
Gao, L., Bowker, M.A., Sun, H., Zhao, J., Zhao, Y., 2020a. Linkages between biocrust development and water erosion and implications for erosion model implementation. Geoderma 357, 113973. https://doi.org/10.1016/j.geoderma.2019.113973.
Gao, L., Sun, H., Xu, M., Zhao, Y., 2020b. Biocrusts resist runoff erosion through direct physical protection and indirect modification of soil properties. J. Soil. Sediment. 20, 133–142. https://doi.org/10.1007/s11368-019-02372-w.
Hamid Lajevardi, S., Shafiei, H., 2023. Investigating the biological treatment effect on fine-grained soil resistance against wind erosion: an experimental case study. Aeolian Res. 60, 100841 https://doi.org/10.1016/j.aeolia.2022.100841.
Havrilla, C.A., Villarreal, M.L., DiBiase, J.L., Duniway, M.C., Barger, N.N., 2020. Ultra-high-resolution mapping of biocrusts with unmanned aerial systems. Remote Sens. Ecol. Conserv. 6, 441–456. https://doi.org/10.1002/rse2.180.
Holt, E.A., Miller, S.W., 2010. Bioindicators: using organisms to measure environmental impacts. Nat. Educ. Knowl. 3, 8.
Houborg, R., McCabe, M.F., 2018. A cubesat enabled spatio-temporal enhancement method (CESTEM) utilizing planet, landsat and MODIS data. Remote Sens. Environ. 209, 211–226. https://doi.org/10.1016/j.rse.2018.02.067.
Housman, D.C., Powers, H.H., Collins, A.D., Belnap, J., 2006. Carbon and nitrogen fixation differ between successional stages of biological soil crusts in the Colorado Plateau and Chihuahuan Desert. J. Arid Environ. 66, 620–634. https://doi.org/10.1016/j.jaridenv.2005.11.014.
Hu, S., Chen, Y., Zhu, H., 2015. Soil infiltration of snowmelt water in the southern Gurbantunggut Desert, Xinjiang, China. J. Appl. Ecol. 26, 1007–1015.
Hu, H., Yang, C.-H.H., Xia, X., Bai, X., Tang, X., Wang, Yajian, Niu, S., Chai, L., Li, J., Zhu, H., Bao, F., Zhao, Y., Siniscalchi, S.M., Wang, Yannan, Du, J., Lee, C.-H., 2021. A two-stage approach to device-robust acoustic scene classification. In: ICASSP 2021–2021 IEEE International Conference on Acoustics, Speech and Signal Processing (ICASSP). Presented at the ICASSP 2021–2021 IEEE International Conference on Acoustics, Speech and Signal Processing (ICASSP). IEEE, Toronto, ON, Canada, pp. 845–849. https://doi.org/10.1109/ICASSP39728.2021.9414835.
Karnieli, A., 1997. Development and implementation of spectral crust index over dune sands. Int. J. Remote Sens. 18, 1207–1220. https://doi.org/10.1080/014311697218368.
Kington, J., Collison, A., 2022. Scene Level Normalization and Harmonization of Planet Dove Imagery. Planet Labs Inc., San Francisco, CA, USA. https://assets.planet.com/docs/scene_level_normalization_of_planet_dove_imagery.pdf.
Knapen, A., Poesen, J., Galindo-Morales, P., Baets, S.D., Pals, A., 2007. Effects of microbiotic crusts under cropland in temperate environments on soil erodibility during concentrated flow. Earth Surf. Process. Landf. 32, 1884–1901. https://doi.org/10.1002/esp.1504.
Lan, S., Wu, L., Zhang, D., Hu, C., 2012. Successional stages of biological soil crusts and their microstructure variability in Shapotou region (China). Environ. Earth Sci. 65, 77–88. https://doi.org/10.1007/s12665-011-1066-0.
Lan, S., Wu, L., Zhang, D., Hu, C., 2013. Assessing level of development and successional stages in biological soil crusts with biological indicators. Microb. Ecol. 66, 394–403. https://doi.org/10.1007/s00248-013-0191-6.
Lan, S., Thomas, A.D., Tooth, S., Wu, L., Hu, C., 2019. Small-scale spatial heterogeneity of photosynthetic fluorescence associated with biological soil crust succession in the Tengger Desert, China. Microb. Ecol. 78, 936–948. https://doi.org/10.1007/s00248-019-01356-0.
Lan, S., Thomas, A.D., Rakes, J.B., Garcia-Pichel, F., Wu, L., Hu, C., 2021. Cyanobacterial community composition and their functional shifts associated with biocrust succession in the Gurbantunggut Desert. Environ. Microbiol. Rep. 13, 884–898. https://doi.org/10.1111/1758-2229.13011.
Latte, N., Lejeune, P., 2020. PlanetScope radiometric normalization and sentinel-2 super-resolution (2.5 m): a straightforward spectral-spatial fusion of multi-satellite multi-sensor images using residual convolutional neural networks. Remote Sens. (Basel) 12, 2366. https://doi.org/10.3390/rs12152366.
Lázaro, R., Gascón, C., Rubio, C., 2023. Runoff and soil loss in biocrusts and physical crusts from the Tabernas Desert (Southeast Spain) according to rainfall intensity. Front. Microbiol. 14, 1171096. https://doi.org/10.3389/fmicb.2023.1171096.
Li, X.R., Jia, X.H., Long, L.Q., Zerbe, S., 2005. Effects of biological soil crusts on seed bank, germination and establishment of two annual plant species in the Tengger Desert (N China). Plant and Soil 277, 375–385. https://doi.org/10.1007/s11104-005-8162-4.
Li, X.R., Chen, Y.W., Su, Y.G., Tan, H.J., 2006. Effects of biological soil crust on desert insect diversity: evidence from the tengger desert of northern China. Arid Land Res. Manag. 20, 263–280. https://doi.org/10.1080/15324980600940985.
Li, Z.Z., Jin, J.H., Liu, R., Xie, X.H., Zou, X.J., Ma, Y.Q., Tan, D.J., 2022. Review and prospect of aeolian geomorphology research in Gurbantunggut Desert, China. J. Desert Res 42 (1), 41–47.
Mutanga, O., Skidmore, A.K., 2004. Hyperspectral band depth analysis for a better estimation of grass biomass (Cenchrus ciliaris) measured under controlled laboratory conditions. Int. J. Appl. Earth Obs. Geoinf. 5, 87–96. https://doi.org/10.1016/j.jag.2004.01.001.
Panigada, C., Tagliabue, G., Zaady, E., Rozenstein, O., Garzonio, R., Di Mauro, B., De Amicis, M., Colombo, R., Cogliati, S., Miglietta, F., Rossini, M., 2019. A new approach for biocrust and vegetation monitoring in drylands using multi-temporal Sentinel-2 images. Progress in Physical Geography: Earth and Environment 43, 496–520. https://doi.org/10.1177/0309133319841903.
Phillips, M.L., McNellis, B.E., Howell, A., Lauria, C.M., Belnap, J., Reed, S.C., 2022. Biocrusts mediate a new mechanism for land degradation under a changing climate. Nat. Clim. Chang. 12, 71–76. https://doi.org/10.1038/s41558-021-01249-6.
Phinney, N.H., Solhaug, K.A., Gauslaa, Y., 2018. Rapid resurrection of chlorolichens in humid air: specific thallus mass drives rehydration and reactivation kinetics.

Environ. Exp. Bot. 148, 184–191. https://doi.org/10.1016/j.envexpbot.2018.01.009.
Planet Team, 2017. Planet Application Program Interface. Space for Life on Earth, San Francisco, CA.
Proctor, M.C.F., Smirnoff, N., 2000. Rapid recovery of photosystems on rewetting desiccation-tolerant mosses: chlorophyll fluorescence and inhibitor experiments. J. Exp. Bot. 51, 1695–1704. https://doi.org/10.1093/jexbot/51.351.1695.
Qiu, D., Bowker, M.A., Xiao, B., Zhao, Y., Zhou, X., Li, X., 2023. Mapping biocrust distribution in China's drylands under changing climate. Sci. Total Environ. 905, 167211 https://doi.org/10.1016/j.scitotenv.2023.167211.
Rabiei, A., Zomorodian, S.M.A., O'Kelly, B.C., 2022. Reducing hydraulic erosion of surficial sand layer by inoculation of cyanobacteria. Proc. Inst. Civ. Eng. Ground Improv. 175, 209–221. https://doi.org/10.1680/jgrim.21.00017.
Reuter, W., Müller, C., 1993. New trends in photobiology. J. Photochem. Photobiol. B Biol. 21, 3–27. https://doi.org/10.1016/1011-1344(93)80159-7.
Rieser, J., Veste, M., Thiel, M., Schönbrodt-Stitt, S., 2021. Coverage and rainfall response of biological soil crusts using multi-temporal sentinel-2 data in a central European temperate dry acid grassland. Remote Sens. (Basel) 13, 3093. https://doi.org/10.3390/rs13163093.
Rivera-Aguilar, V., Godínez-Alvarez, H., Manuell-Cacheux, I., Rodríguez-Zaragoza, S., 2005. Physical effects of biological soil crusts on seed germination of two desert plants under laboratory conditions. J. Arid Environ. 63, 344–352. https://doi.org/10.1016/j.jaridenv.2005.03.012.
Rodríguez-Caballero, E., Escribano, P., Cantón, Y., 2014. Advanced image processing methods as a tool to map and quantify different types of biological soil crust. ISPRS J. Photogramm. Remote Sens. 90, 59–67. https://doi.org/10.1016/j.isprsjprs.2014.02.002.
Rodríguez-Caballero, E., Belnap, J., Büdel, B., Crutzen, P.J., Andreae, M.O., Pöschl, U., Weber, B., 2018. Dryland photoautotrophic soil surface communities endangered by global change. Nat. Geosci. 11, 185–189. https://doi.org/10.1038/s41561-018-0072-1.
Román, J.R., Rodríguez-Caballero, E., Rodríguez-Lozano, B., Roncero-Ramos, B., Chamizo, S., Águila-Carricondo, P., Cantón, Y., 2019. Spectral response analysis: an indirect and non-destructive methodology for the chlorophyll quantification of biocrusts. Remote Sens. (Basel) 11, 1350. https://doi.org/10.3390/rs11111350.
Sancho, L.G., Belnap, J., Colesie, C., Raggio, J., Weber, B., 2016. Carbon budgets of biological soil crusts at micro-, meso-, and global scales. In: Weber, B., Büdel, B., Belnap, J. (Eds.), Biological Soil Crusts: An Organizing Principle in Drylands. Springer International Publishing, Cham, pp. 287–304.
Smith, W.K., Dannenberg, M.P., Yan, D., Herrmann, S., Barnes, M.L., Barron-Gafford, G. A., Biederman, J.A., Ferrenberg, S., Fox, A.M., Hudson, A., Knowles, J.F., MacBean, N., Moore, D.J.P., Nagler, P.L., Reed, S.C., Rutherford, W.A., Scott, R.L., Wang, X., Yang, J., 2019. Remote sensing of dryland ecosystem structure and function: Progress, challenges, and opportunities. Remote Sens. Environ. 233, 111401 https://doi.org/10.1016/j.rse.2019.111401.
Sun, Y., Babbs, C.F., Delp Iii, E.J., 2004. A two-stage classifier system for normal mammogram identification. In: Bouman, C.A., Miller, E.L. (Eds.), Presented at the Electronic Imaging 2004, San Jose, CA, p. 112. https://doi.org/10.1117/12.538996.
Tian, C., Pang, J., Bu, C., Wu, S., Bai, H., Li, Y., Guo, Q., Siddique, K.H.M., 2023. The microbiomes in lichen and moss biocrust contribute differently to carbon and nitrogen cycles in arid ecosystems. Microb. Ecol. 86, 497–508. https://doi.org/10.1007/s00248-022-02077-7.
Wang, Y., 1993. Phenological observation of the early spring ephemeral and ephemeroid plant in Xinjiang. Arid Zone Res. 10, 34–39.
Wang, Z., Wu, B., Zhang, M., Zeng, H., Yang, L., Tian, F., Ma, Z., Wu, H., 2022. Indices enhance biological soil crust mapping in sandy and desert lands. Remote Sens. Environ. 278, 113078 https://doi.org/10.1016/j.rse.2022.113078.
Wang, Z., Wu, B., Ma, Z., Zhang, M., Zeng, H., Yang, L., 2023. Spectral determinants of biological soil crusts in the Gurbantungut Desert. Int. J. Remote Sens. 44, 2273–2293. https://doi.org/10.1080/01431161.2023.2198653.
Weber, B., Bowker, M., Zhang, Y., Belnap, J., 2016. Natural recovery of biological soil crusts after disturbance. In: Weber, B., Büdel, B., Belnap, J. (Eds.), Biological Soil Crusts: An Organizing Principle in Drylands. Springer International Publishing, Cham, pp. 479–498.
Wu, L., Zhang, Y.M., 2013. Coverage estimation on biological soil crusts based on digital photos. J. Desert Res. 33, 1810–1815.
Wu, L., Rossi, F., Lan, S., 2023. Potential mechanisms of soil nitrogen content heterogeneity associated with biocrust development in drylands. Eur. J. Soil Sci. 74, e13429 https://doi.org/10.1111/ejss.13429.
Yair, A., Almog, R., Veste, M., 2011. Differential hydrological response of biological topsoil crusts along a rainfall gradient in a sandy arid area: northern Negev Desert, Israel. CATENA 87, 326–333. https://doi.org/10.1016/j.catena.2011.06.015.
Yamano, H., Chen, J., Zhang, Y., Tamura, M., 2006. Relating photosynthesis of biological soil crusts with reflectance: preliminary assessment based on a hydration experiment. Int. J. Remote Sens. 27, 5393–5399. https://doi.org/10.1080/01431160600823214.
Yang, K., Zhao, Y., Gao, L., 2022. Biocrust succession improves soil aggregate stability of subsurface after "Grain for Green" Project in the Hilly Loess Plateau, China. Soil Tillage Res. 217, 105290 https://doi.org/10.1016/j.still.2021.105290.
Zeng, Y., Hao, D., Huete, A., Dechant, B., Berry, J., Chen, J.M., Joiner, J., Frankenberg, C., Bond-Lamberty, B., Ryu, Y., Xiao, J., Asrar, G.R., Chen, M., 2022. Optical vegetation indices for monitoring terrestrial ecosystems globally. Nat. Rev. Earth Environ. 3, 477–493. https://doi.org/10.1038/s43017-022-00298-5.
Zhang, Y., Wu, N., Zhang, B., Zhang, J., 2010. Species composition, distribution patterns and ecological functions of biological soil crusts in the Gurbantunggut Desert. J. Arid. Land 2, 180–189. https://doi.org/10.3724/sp.j.1227.2010.00180.
Zhao, Y., Qin, N., Weber, B., Xu, M., 2014. Response of biological soil crusts to raindrop erosivity and underlying influences in the hilly Loess Plateau region, China. Biodivers. Conserv. 23, 1669–1686. https://doi.org/10.1007/s10531-014-0680-z.
Zhou, H.F., Li, Y., Tang, Y., Zhou, B.J., Xu, H.W., 2010. The characteristics of the snow-cover and snowmelt water storage in Gurbantunggut Desert. Arid Zone Res. 26, 312–317. https://doi.org/10.1007/s10531-014-0680-z.
Zomer, R.J., Xu, J., Trabucco, A., 2022. Version 3 of the global aridity index and potential evapotranspiration database. Scientific Data 9, 409. https://www.nature.com/articles/s41597-022-01493-1.